Human Movement Science 64 (2019) 252–273

Contents lists available at ScienceDirect

Human Movement Science

journal homepage: www.elsevier.com/locate/humov

Dynamic simulation of flat water kayaking using a coupled biomechanical-smoothed particle hydrodynamics model

Simon M. Harrison*, Paul W. Cleary, Raymond C.Z. Cohen

CSIRO Data61, Australia

ARTICLE INFO

Keywords:
Smoothed particle hydrodynamics (SPH)
Canoe
Computational fluid dynamics (CFD)
Biomechanics
Kayak

ABSTRACT

Kayak racing performance is known to be dependent on technique, strength and equipment, but the relationship between these factors and performance is not well understood. Complete experimental measures of stroke technique and the interactions between the water and the paddle and the boat are not practical in a racing environment. Instead, simulation using computational fluid dynamics can be used to study this system. A coupled biomechanical-Smoothed Particle Hydrodynamics (B-SPH) model of the kayaking athlete is presented. Verification and validation of the model are confirmed using drag force data from the literature and a spatial resolution study. Using this model and stroke kinematics (developed from the combination of literature data and digitised motion of an amateur level athlete from video), calculations are made of (a) the fluid response to interactions with the paddle and kayak; (b) speed of the kayak; and (c) magnitudes of force and impulse on the paddle and the hands. Key features of the fluid response are related to the loading on the athlete and the speed of the kayak. Perturbations to stroke technique are explored to give new insights into the relationships between technique and racing performance.

1. Introduction

Kayak and rowing racing performance is known to depend on athlete attributes such as aerobic and anaerobic capacities (Bishop, 2000), anthropometry (Van Someren & Howatson, 2008; Van Someren & Palmer, 2003), strength and stroke technique (Buckeridge, Bull, & McGregor, 2014; McDonnell, Hume, & Nolte, 2013; McKean & Burkett, 2010; Michael, Smith, & Rooney, 2009), and also on both boat and blade design (Michael et al., 2009). The dynamic interactions between water and the hull and blade have been described qualitatively (Jackson, 1995; Michael et al., 2009). However, quantification of the relationship between these factors and the speed of the boat has not yet been achieved. Analyses of measurable physiological differences between athletes (Fry & Morton, 1991; Olivier & Coetsee, 2002; Van Someren & Howatson, 2008; Van Someren & Palmer, 2003) and/or laboratory based performance measures on an ergometer (Fry & Morton, 1991) have been used to enhance understanding of the basis of performance outcomes. But, they cannot directly predict speed changes due to variations of stroke technique or equipment design without recalibrating the model parameters using specific experiments for each new case. Also, they cannot provide insight into the biomechanical causes of varied performance either between athletes with different attributes or for the same athlete with varied equipment, or changes to the athlete's ability over time (such as the effects of altered training and strengthening programs or the effects of injury).

A dynamic computational model of kayaking that incorporates biomechanical and fluid dynamics model components can add new understanding to the relationships between racing speed and changes to technique, physiology and/or equipment. For example,

* Corresponding author at: CSIRO Data61, Private Bag 33, Clayton South, VIC 3169, Australia.
E-mail address: Simon.Harrison@csiro.au (S.M. Harrison).

https://doi.org/10.1016/j.humov.2019.02.003
Received 3 October 2018; Received in revised form 6 February 2019; Accepted 13 February 2019
Available online 26 February 2019

stroke technique is known to be different for elite and sub-elite athletes (Limonta et al., 2010), though it is not yet known how specific changes to technique for individual athletes will affect performance. Computational modelling provides control of one or more parameters which are much more difficult or impossible to control in a physical experiment. This enables more careful investigation of the effect of changes to factors such as stroke symmetry or stroke rate on racing speed and loading on the athlete's body. Such studies can be used to:

1. Gain insight into how fundamental variables (e.g. stroke rate, stroke symmetry, equipment attributes, endurance) affect racing speed.
2. Predict racing speed and loading on the body for an individual athlete for
   a. a proposed change to technique; and
   b. a proposed change to strength and conditioning training.

These model results would contribute to the body of knowledge in the area and could assist future training decisions.

Computational simulation of water-based sports presents significant modelling challenges. In kayaking the boat hull translates and rotates substantially and the paddle blade moves and rotates in complicated motions as it interacts with the free surface of the water. In response, the surface of the water experiences large displacements and fragmentation, or splashing. Smoothed Particle Hydrodynamics (SPH) is a Lagrangian particle method that is well suited to such transient fluid problems with moving boundaries possessing complicated shape. Recent work in swimming (Cleary et al., 2013; Cohen, Cleary, & Mason, 2012; Cohen, Cleary, Mason, & Pease, 2015, 2018) and platform diving (Harrison, Cohen, Cleary, Barris, & Rose, 2016) has shown the viability and usefulness of this method for simulation and biomechanical analysis of aquatic sports.

We present a coupled biomechanical-smoothed particle hydrodynamics (B-SPH) modelling framework for the performance prediction of kayak racing. Three dimensional representations of the kayak and paddle geometries and a detailed representation of athlete stroke technique are coupled to an SPH representation of the water dynamics. The model can predict the complete dynamic behaviour of the water, athlete, kayak and paddle, and the forces exerted on the kayak hull, the paddle and by each hand on the paddle. This allows variation of stroke technique, athlete anthropometry and equipment (i.e. geometry and mass of the kayak and paddle) to be simulated. Model results are verified by a particle resolution study and validated against published data. The aim of this paper is to detail the modelling method used and show the utility of the model for investigating changes to technique and equipment. In this first demonstration of the model we investigate the variation to kayak speed and the loading on the paddle and hands:

1. due to variations in stroke rate; and
2. due to variations in the depth of the right stroke through the water;

using generic equipment designs and stroke techniques.

2. Computational model

The computational model is comprised of three coupled sub-models

1. a biomechanical model of the athlete, which relates the skeletal kinematics of the athlete to the instantaneous conformation of their skin surface and the position of the paddle in the local coordinate frame of the athlete;
2. a computational fluid dynamics model, using SPH, that describes dynamics of the water including free surface behaviour and splashing; and
3. a coupling treatment of the fluid-structure interactions between
   a. the water and the kayak and paddle blade (and athlete if contact is made)
   b. the athlete and the kayak

To understand the dynamic behaviour of the athlete, kayak and water and the forces transmitted between them, we introduce three coordinate frames: the local frame of the athlete called RF2 (Fig. 1a) in which the stroke technique is represented and which has its origin at the athlete's centre of mass (CoM); the local frame of the kayak that has its origin at the centre of mass of the kayak called RF3 (Fig. 1b), and the world coordinate frame, called RF1, in which the interactions between the water and the blade and kayak are calculated (Fig. 1c).

Here we detail the basis of each model and the coupling between them.

2.1. Biomechanical model of the athlete and equipment

2.1.1. Dynamic skeletal linkage model of the body

The athlete was represented in the computational model by a deforming three dimensional surface mesh. A generic 1.8 m tall male adult geometry was used. The athlete mesh (Fig. 1a) used had 58,000 nodes, spaced at an average separation of 10 mm. The model athlete's skeleton comprised 23 spherical joints, which represent the major articulations of the body (ankles, knees, hips, back, shoulders, neck, elbows, wrist etc.) (Anderson & Pandy, 1993). An individual pose of the skeleton in the athlete coordinate frame is specified by a set of three joint angles for each of these 23 spherical joints. A mass of 80 kg was assumed for calculations of the

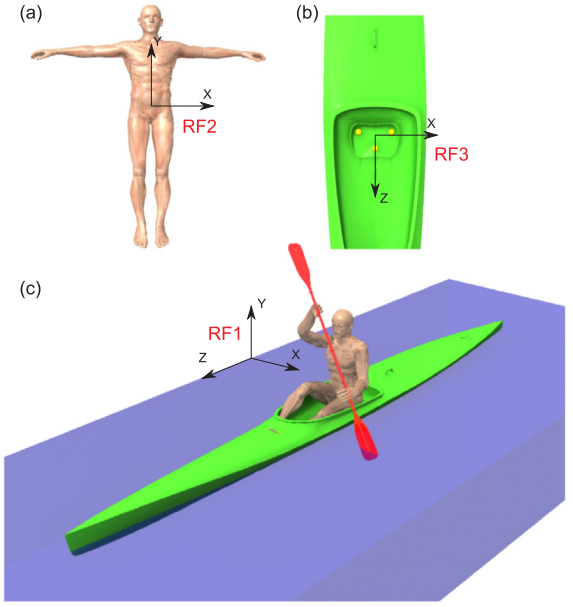

Fig. 1. (a) The mesh model of the athlete, showing its reference frame (RF3); (b) close up view of the kayak mesh model at the seat, showing the kayak reference frame (RF3) and the locations of the springs that connect the athlete's surface to the kayak frame (yellow spheres); and (c) the complete athlete-paddle-kayak model showing the placement of the paddle in the hands of the athlete, the tank of water and the world reference frame (RF1). (For interpretation of the references to colour in this figure legend, the reader is referred to the web version of this article.)

dynamic movement of the model athlete's body.

The movement and deformation of the skin surface of the athlete was calculated from the movement of the skeleton using a skin rigging method. This skin rigging was performed using the dual quaternion method (Kavan, Collins, Zára, & O'Sullivan, 2008). Each vertex of the mesh translates according to the motion of between 1 and 5 nearby joints in manner that represents soft tissue deformation during movement (Cohen et al., 2012, 2014).

2.1.2. Representations of the kayak and paddle

A 6.0 m long, 0.6 m wide, 0.35 deep flat water (K1) kayak was used in this study (Fig. 1b and c). Such a kayak would usually have 165 mm of its depth submerged below the surface of the water at rest. For indicative race conditions on water, the Reynolds number (Re), based on length, would be of the order 10^7 and the Froude number (Fr), based on kayak length, would be of the order of 0.625. From this, Jackson (1995) estimated the corresponding wave drag force on the K1 kayak at racing speed (4.83 m/s) to be 17.1 N, which is 21% of the total drag force. The surface of the kayak was represented in three dimensions by a surface mesh of approximately 102,000 nodes with an average spacing of 10 mm.

A flat kayak paddle of length 1.92 m (with each paddle blade of length 435 mm, width 166 mm and thickness 5 mm) was represented as mesh of 1,200 nodes, also with an average spacing of 10 mm. The paddle blade is submerged for between 0.1 s and 0.2 s during racing. An average resolution of 10 mm was sufficient to represent the key features of the object geometries with finer resolution used where required to accurately represent smaller features, e.g. through the thickness of the paddle blade.

Mathematical constraints are used to couple the dynamics of the kayak hull to the athlete's body. Contact between, the athlete model and the kayak seat is modelled using three zero-length springs located in an equilateral triangle (Fig. 1b), in the horizontal plane at the seat. The compliance of the soft tissue in the seat of the athlete is represented by using a spring stiffness of 50 kN/m. Using this approach, movement of the kayak due to hull-water interactions are transmitted to the athlete model component and the forces from the paddle are transmitted through the athlete to the kayak.

2.1.3. Kinematics digitisation

A symmetric stroke technique was digitised from the combination of video footage of an amateur athlete (Eddy, 2011) and kinematic data from Limonta et al. (2010). Each of the individual frames of the 30 Hz video footage was extracted for the digitisation process. The athlete model was posed in the computational model by manipulation of the 23 skeletal joints to match the pose of the athlete in each video frame over one stroke cycle. As the movement out of plane of the video frame was not precisely known, the motion components in the plane orthogonal to the view in the video footage were specified using data from kinematic studies (Limonta et al., 2010) to reflect the stroke style of an elite athlete. The trajectories of the wrists and the tips of the paddle blade of the athlete model performing the digitised motion are shown in Fig. 2.

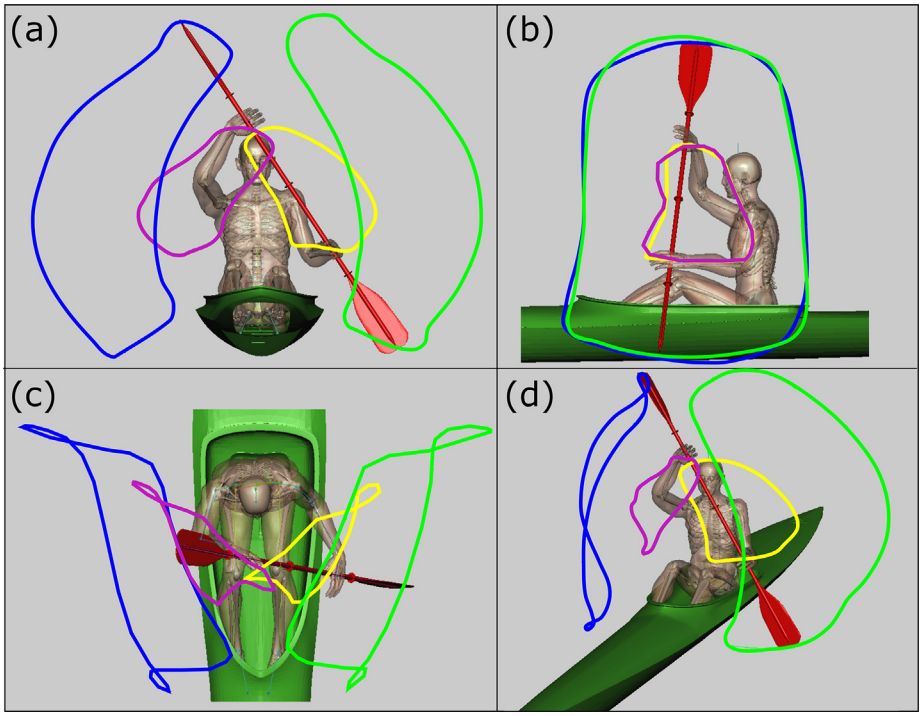

Fig. 2. Motion trails of the left and right tips of the kayak blade (blue and green respectively) and the left and right wrist (purple and yellow respectively) from (a) front, (b) side, (c) top and (d) oblique views. (For interpretation of the references to colour in this figure legend, the reader is referred to the web version of this article.)

2.2. SPH method for fluid simulation

SPH is a mesh-free Lagrangian particle method for solving partial differential equations that is particularly suitable for modelling aquatic sports. The method has been broadly adopted for problems involving complex free surface hydrodynamics and interaction of fluids with structures. It was introduced by Monaghan (1994), and has been used for applications as diverse as die casting (Cleary, Ha, & Ahuja, 2000; Ha & Cleary, 2005), slurry transport (Cleary, Sinnott, & Morrison, 2006), muddy debris flow (Pasculli, Minatti, Audisio, & Sciarra, 2014), dam collapse and tsunamis (Cleary & Prakash, 2004), wave impact on oil platforms (Cleary & Rudman, 2009) and other structures (Crespo, Gómez-Gesteira, & Dalrymple, 2007; Gómez-Gesteira & Dalrymple, 2004), human mastication (Harrison & Cleary, 2014), fluid sloshing (Rudman, Cleary, & Prakash, 2009) and fluid-structure interaction (Cummins, Silvester, & Cleary, 2012). Monaghan (2005), Cleary, Prakash, Ha, Stokes, and Scott (2007a) and Liu and Liu (2010) provide good summaries of many applications.

In SPH, volumes of fluid are represented by a moving set of particles, on which the Navier-Stokes equations can be reduced to the following ordinary differential equations:

$$\frac{d\rho_a}{dt} = \sum_b m_b \boldsymbol{v}_{ab} \cdot \nabla_a W_{ab} \tag{1}$$

where ρ_a is the density of particle a, t is time, m_b is the mass of particle b, where $\mathbf{v}_{ab} = \mathbf{v}_a - \mathbf{v}_b$ and $\mathbf{v}_a$ and $\mathbf{v}_b$ are the velocities of particles a and b. W is an interpolation kernel function that is evaluated for the distance between particles a and b. This kernel function (in this case a cubic spline) allows for interpolation of all particle states (e.g. position, velocity, temperature etc.) across the volume occupied by particles. The smoothing length of the kernel, h, is chosen to be $1.2p$, where p is the spacing of the fluid particles. The kernel diameter for the cubic spline kernel of Monaghan (1994) is $2h$:

$$\frac{d\boldsymbol{v}_a}{dt} = \mathbf{g} - \sum m_b \left[\left(\frac{P_b}{\rho_b^2} + \frac{P_a}{\rho_a^2} \right) - \frac{\xi}{\rho_a \rho_b} \frac{4\mu_a \mu_b}{(\mu_a + \mu_b)} \frac{\boldsymbol{v}_{ab} \cdot \boldsymbol{r}_{ab}}{\boldsymbol{r}_{ab}^2 + \eta^2} \right] \nabla_a W_{ab} \tag{2}$$

where P_a and μ_a are the local pressure and dynamic viscosity for particle a, η is a small number to mitigate singularities, ζ is a normalisation constant for the kernel function and $\mathbf{g}$ is the gravitational acceleration.

A quasi-compressible formulation of the SPH method is employed with an equation of state relating the fluid pressure, P to the particle density, ρ:

$$P = P_0\left[\left(\frac{\rho}{\rho_0}\right)^{\gamma} - 1\right] \tag{3}$$

where P_0 prescribes the overall dynamic pressure scale and the reference density is given by ρ_0. γ is a material constant, which is equal to 7 for fluids with compressibility properties similar to water (Batchelor, 1973).

The equations of motion for the particles (1) and (2) are integrated using a second order predictor-corrector (see Monaghan, 1994 for details). The limit for stable integration is given by the Courant condition modified for viscosity (see Monaghan, 1994; Cleary, 1998). The integration is stable with a timestep:

$$\delta t = \min_a\left[\frac{h}{2\left(c + \frac{2\xi\mu_a}{h\rho_a}\right)}\right] \tag{4}$$

where the minimum is over all SPH fluid particles and c is the numerical speed of sound:

$$\frac{\gamma P_0}{\rho_0} = 100V^2 = c^2 \tag{5}$$

is ten times the characteristic maximum speed of the flow V and is related to the pressure scale P_0. This ensures that density variations are sufficiently small for the flow to be regarded as incompressible.

The SPH software used in this work is developed in-house by CSIRO and has been used extensively for industrial, geophysical and biophysical applications (see Cleary et al., 2000, 2006a, 2006b, 2007aCleary et al., 2013; Cleary & Prakash, 2004; Ha & Cleary, 2005; Cleary & Rudman, 2009; Cohen et al., 2012, 2015, 2018; Cummins et al., 2012; Harrison & Cleary, 2014; and Harrison et al., 2014). Specific validation of fluid flow predictions of this solver have been performed with good agreement or better for die casting (Cleary, Ha, Prakash, & Nguyen, 2006a; Ha & Cleary, 2000), impact of a breaking wave against a column (Cummins et al., 2012), sloshing in a tank (Rudman et al., 2009), mixing (Prakash, Cleary, Noui-Mehidi, Blackburn, & Brooks, 2007; Robinson, Cleary, & Monaghan, 2008). Specific verification of solution accuracy has been performed using Couette flow (Cleary, 1996) and a Backward Facing Step problem (Ting, Prakash, Cleary, & Thompson, 2006).

For such an application, the flow cannot be characterised by a single Re. For the flow around the hull, Re is of the order of 10^7 meaning that the flow will have turbulent structures generated around the kayak. The situation for the blade is more complex due to the short interval over which it is submerged during each stroke (order 0.2 s) with a peak Re of order 10^5 (assuming a characteristic length of 0.1 m). This Re is smaller due to the much smaller characteristic size of the paddle. Since turbulent structures take time to develop, the limited duration of submersion and the varying speed of the blade mean that the ability to generate substantial turbulent structure from the blade is limited. These combined with the moderate transitional Re means that turbulence is less critical for the blade than for the hull.

The SPH method is constructed by applying a spatial filtering to the original governing partial differential equations. This filtering is of the same form as used in the construction of Large Eddy Simulation (LES) methods. Essentially, SPH attempts to resolve all of the structures whose scales are larger than the interpolation length h and relies on sub-grid scale models (for example see Ting et al., 2006) or numerical diffusion (Cleary et al., 2007a) to dissipate energy cascading down from larger scale to the unresolved scales. If energy travels rather from small scales up to large scales to create coherent structures then the SPH method has difficulties in achieving this due to numerical diffusion arising from the tensile instability on scales just above the interpolation length scale (Robinson & Monaghan, 2012). However, for this application energy is transferred from the blade to the water generating vortex structures with larger scales that can be adequately resolved. The subsequent break-up behaviour of these large initial vortices can no longer influence the blade and boat drag and propulsion once they move away from these surfaces and no longer interact. So resolution of all finer turbulent structure is not critical for this application. The adequacy of this assumption is demonstrated both by the validation test cases that follow and the small variation observed in the predicted equilibrium boat speed with increasing resolution.

2.3. Adequacy of the resolution of the kayak blade

The discretisation resolution means that there are approximately 11 boundary particles across the width of the blade and 34 particles from the tip to the start of the blade. This is more than sufficient to resolve the normal stress distribution on the blade. The blade depth at 13 mm is small compared to the fluid particle resolution. This has no effect on the normal component of flow and forces around the blade, but can affect the accuracy of the shear forces. Without a special treatment for the thinness of the blade, the fluid on the front of the blade can feel some viscous effects from both the back and front of the blade. The force interpolation is over $2.4p$ which is 36 mm for a fluid resolution of 15 mm. If the blade is thicker than $0.4p$ then the fluid on one side is beyond the interpolation distance of the fluid on the other side. For a fluid resolution of 15 mm the blade thickness (13 mm) is larger than this fluid overlap distance (6 mm). The inclusion of both the front and back of the blade in the shear force calculation means that there is some numerical diffusion in the shear direction resulting from the thinness of the blade. Since the kernel is approximately Gaussian and declines rapidly with distance this effect is small. The angle of attack of the blade during a stroke is such that the flow forces applied at the blade surface are predominantly normal to the blade. The shear forces at the blade surface are relatively lower. The combination of the relatively lower importance of the blade shear forces in this application with the fast drop-off of the shear force

interpolation with distance means that the resulting numerical diffusion from the thin blade structure is relatively small. This approximation is acceptable for the current modelling purposes. The effect of this numerical diffusion on the solution accuracy around the blade will be tested in Section 3 to verify that it is not significant.

2.4. Three dimensional vortex identification

The dynamics and evolution of large scale coherent vortex structures play an important role in the transport of momentum in many different flows (Farahani & Dalrymple, 2014). As the paddle blade passes through the water it generates a U-shaped vortex (Jackson, Locke, & Brown, 1992). The work done by the blade and the impulse during the stroke provide energy and impulse to the water which is indicated by this vorticity. Thus visualisation of the vortex characteristics can be used to assess (and quantify) the effectiveness of the paddle stroke.

Three-dimensional vortex wake structures are identified using the λ_2 method described by Jeong and Hussain (1995). In this method a vortex said to occur at local pressure minimums which corresponds to when there are two negative eigenvalues ($\lambda_1 \leq \lambda_2 \leq \lambda_3$ and $\lambda_2 < 0$) of $\mathbf{S}^2 + \Omega^2$, where $\mathbf{S}$ and Ω are the symmetric and anti-symmetric components of the velocity gradient tensor, $\nabla \boldsymbol{v}$. SPH results are mapped onto a uniform grid and the eigenvalues of $\mathbf{S}^2 + \Omega^2$ are calculated at each grid point using the SPH gradient operator. Iso-surfaces of $\lambda_2 = -\epsilon$ (where ϵ is a small value) are generated for visualisation of outer surfaces of the three dimensional vortex structures. Farahani and Dalrymple (2014) previously used the λ_2 method in their SPH studies of coherent structures in breaking waves.

2.5. Treatment of boundaries and fluid-structure interactions

Interactions between the fluid and the objects (i.e. kayak and paddle) are treated using boundary SPH particles at each node of the object mesh. A Lennard-Jones type penalty force is applied at each boundary particle in contact with fluid. The penalty force replaces the pressure force terms in the momentum Eq. (2) for moving particle-solid node pairs. Non-slip boundary conditions in the directions tangential to the solid surfaces are generated by including the fluid-solid pairs in the summations for the viscous stress in Eq. (2). This is a flexible boundary implementation that allows very complex solid boundaries (Cleary et al., 2006; Cleary et al., 2006), moving boundaries (Cleary et al., 2007a) and deforming boundaries (Cohen et al., 2012) to be modelled. For deforming bodies such as the athlete, the nodal positions and the normal vectors are updated at each time-step to reflect the current shape of the surface.

Movement of the kayak, paddle and athlete is calculated from fluid, inertia and gravity forces by solving Newton's equations of motion. The moments of inertia of the objects were calculated from their mass, geometric structure and pose, assuming a homogeneous distribution of density around their centre of mass. The force, $\mathbf{f_{obj}}$, acting on each object mesh (paddle or kayak hull) from the water is calculated by summing the individual boundary particle forces, $\mathbf{f_i}$:

$$\boldsymbol{f}_{\boldsymbol{obj}} = \sum_{i=1}^{M} \boldsymbol{f}_{\boldsymbol{i}} \tag{6}$$

where M is the number of boundary particles that comprise the object boundary mesh. SPH has been shown to provide robust and accurate calculations of force for situations where boundaries interact with the fluid free surface using this method (Cummins et al., 2012).

The torque, $\mathbf{T_{obj}}$, on each object from the water was calculated as the sum of the torques applied at each boundary particle of each surface mesh. The torque at each boundary particle is given by the cross product of each boundary force, $\mathbf{f_i}$, with the corresponding position vector of the boundary particle, $\mathbf{r_i}$, relative to the object CoM:

$$\boldsymbol{T}_{\boldsymbol{obj}} = \sum_{i=1}^{M} \boldsymbol{r}_{\boldsymbol{i}} \times \boldsymbol{f}_{\boldsymbol{i}} \tag{7}$$

For each time step these net forces and torques are the source terms in Newton's equation and the corresponding equation for the spin of each of the objects (kayak, paddle and athlete). These are integrated using a second order improved-Euler scheme to give the new velocity and spin of the object. The kinematic equations are then similarly integrated to give the new position and orientation of the mesh. The motion of the kayak is determined by the magnitude of propulsive and drag forces that occur during paddle-water interactions and drag forces on the kayak hull (from friction, pressure and wave drag, see Jackson (1995) and Michael et al. (2009)).

Typically an athlete will control the rotation of the paddle about its longitudinal axis with one hand (Mann & Kearney, 1979). The hand closest to the submerged blade is the thrust hand and pulls the blade towards the stern. The other hand is the draw hand, which pushes towards the bow, counteracting the torque that is generated by the blade-water interaction. The loading on the hands in the model was calculated by assuming that the hands act as mechanical joints connected to the paddle. The left hand was specified as a three angular degree of freedom joint because the athlete allows the paddle to rotate in their left hand. The right hand was specified as a two angular degree of freedom joint because the athlete does not allow the paddle to rotate in this hand. The force on the thrust and draw hand, $\mathbf{f_{thrust}}$ and $\mathbf{f_{draw}}$ respectively, were calculated from two simultaneous equations: the sum of the forces and the sum of the torques on the paddle:

$$\boldsymbol{f}_{\boldsymbol{thrust}} + \boldsymbol{f}_{\boldsymbol{draw}} = m_{paddle}\boldsymbol{a}_{\boldsymbol{paddle}} - \boldsymbol{f}_{\boldsymbol{paddle}} \tag{8}$$

$$\boldsymbol{u}_{thrust} \times \boldsymbol{f}_{thrust} + \boldsymbol{u}_{draw} \times \boldsymbol{f}_{draw} = \boldsymbol{I}_{paddle}\boldsymbol{\alpha}_{paddle} - \boldsymbol{u}_{paddle} \times \boldsymbol{f}_{paddle} - \boldsymbol{T}_{right} \quad (9)$$

where m_{paddle} is the mass of the paddle, $\mathbf{a}_{\mathbf{paddle}}$ is its acceleration, $\mathbf{I}_{\mathbf{paddle}}$ is its moment of inertia matrix and $\alpha_{\mathbf{paddle}}$ is its rotational acceleration. The distance of the hands and fluid force contributions on the blade from its centre of mass are denoted by $\mathbf{u}_{\mathbf{left}}$, $\mathbf{u}_{\mathbf{right}}$ and $\mathbf{u}_{\mathbf{paddle}}$ respectively. The torque about the longitudinal axis of the blade exerted by the right hand is $\mathbf{T}_{\mathbf{right}}$ and is calculated using Eq. (7). The acceleration terms $\mathbf{a}_{\mathbf{paddle}}$ and $\alpha_{\mathbf{paddle}}$ are calculated from the known body kinematics and the acceleration of the athlete (and kayak) with respect to the water from the SPH solution:

$$\boldsymbol{a}_{paddle} = \boldsymbol{a}_{paddle-athlete} + \boldsymbol{a}_{paddle-water} \quad (10)$$

$$\boldsymbol{\alpha}_{paddle} = \boldsymbol{\alpha}_{paddle-athlete} + \boldsymbol{\alpha}_{athlete-water} \quad (11)$$

where the linear and rotational accelerations of the paddle with respect to the athlete are $\mathbf{a}_{\mathbf{paddle\text{-}athlete}}$ and $\alpha_{\mathbf{paddle\text{-}athlete}}$ respectively, and the linear and rotational accelerations of the athlete with respect to the water are $\mathbf{a}_{\mathbf{athlete\text{-}water}}$ and $\alpha_{\mathbf{athlete\text{-}water}}$ respectively.

Reported forces and torques were smoothed using a top hat averaging technique, with a filter width of 10 time steps (of period 0.3 ms). The impulse was calculated per stroke as the integral of force with time.

2.5.1. Variants of stroke rate and style

Racing stroke rates are typically 110–120 SPM and sprinting stroke rates can be 135 SPM or higher (Baker, Rath, Sanders, & Kelly, 1999; Qiu, Wei, Liu, & Cao, 2008). While it is known that increased stroke rate results in faster speeds, it has not been quantified how a faster stroke rate increases speed or how it affects the loading on the paddle and hands. The digitised technique (at 95 SPM) was uniformly scaled in time to produce stroke rates of 115 and 135 SPM, retaining the relativity of the different stroke elements, to represent racing and sprint stroke styles respectively.

Differences in stroke technique between elite and amateur athletes are numerous but are not consistent across a number of studies (Helmer, Farouil, Baker, & Blanchonette, 2011; Limonta et al., 2010). However, left-right asymmetry of the paddle blade tip trajectory is the most common and significant reported difference. To study the impact of this difference between elite and non-elite athletes, we considered two additional sets of stroke kinematics. In the first, Asymm1, the maximum depth of the tip of the blade under the water during the right side stroke was reduced by 4.7 cm (to 58% of the original stroke depth) and by 7.2 cm in the second case, Asymm2, (to only 36% of the original stroke depth). The left side stroke was unchanged in both cases, making this the dominant side. The resulting asymmetric stroke kinematics was used to assess the changes in kayak motion and paddle force due to alterations in left-right stroke depth symmetry. The aim is both to better understand the consequences of asymmetry of the stroke and to demonstrate how such a computational model can be used to understand relative performance of different scenarios.

2.5.2. Initial conditions

The flat water racing environment was modelled by an initially stationary volume of water 1 m deep (Y direction), 3 m wide (Z direction) and 40 m long (X direction). These dimensions are sufficient to ensure that the simulation predictions are independent of the choice and not influenced by edge effects from the sides of the domain. The water was represented by 37 million SPH particles with a separation of 15 mm. Periodic boundary conditions were used in both horizontal directions to represent a larger volume of river or lake. This is the simplest way when using SPH to minimise disturbances from the edges of the domain on the flow in the vicinity of the kayak. The base of the river/lake was modelled as a static set of boundary particles. The dynamic viscosity (μ) of the water was 1.4×10^{-3} Pa s. The kayak was initially positioned with its CoM at X = 2.5 m, Z = 0 m in the world coordinate frame (RF1 in Fig. 1) and at the vertical position corresponding to equilibrium position where buoyancy and gravity forces are in balance.

Table 1 shows a summary of all simulation cases and the initial kayak speed used in each. In Section 4 we investigate the acceleration of the kayak to equilibrium speed at the stroke rate of 135 S per minute (135SPMAcc). The initial kayak speed was set at a suitable speed to achieve equilibrium speed within six strokes. In Section 5 we study the effect of stroke rate on hull and water dynamics at equilibrium speed (cases 95SPM, 115SPM and 135SPM). For these, the initial kayak speed was set at a suitable speed to achieve equilibrium speed within two strokes. In Section 6 we compare the model results for variations in left-right symmetry of stroke (cases 135SPMAcc, Asymm1, and Assym2). The initial kayak speed for these was same for each case and set as the speed required to achieve equilibrium speed within six strokes for the symmetric case (135SPM).

Table 1
Stroke rate, initial kayak speed and symmetry of stroke used in the simulation cases.

Name	Stroke rate (min^{-1})	Initial kayak speed (m/s)	Left/Right Symmetric?
135SPMAcc	135	4.9	Yes
135SPM	135	5.0	Yes
115SPM	115	4.0	Yes
95SPM	95	3.0	Yes
Asymm1	135	5.0	Right side depth = 58% of the left side depth
Asymm2	135	5.0	Right side depth = 36% of the left side depth

2.6. Analysis of model outputs

The motions of the kayak, athlete and water are dynamic and as a result the evaluation of kayaker performance requires further analysis than just the prediction of temporal variation of velocities and forces. There are two types of transient motion: (1) the variations in forwards speed that occur with each stroke (Gomes et al., 2011; Janssen & Sachlikidis, 2010), and (2) the acceleration of the kayak from a stationary position to racing speed. Two types of averaging are used in this study to enable comparison:

1. Between stroke averaging (BSA)
2. Within stroke averaging (WSA)

For BSA an individual result at a specific phase of stroke is averaged over multiple strokes, which reduces noise from transient movements of the kayak and water. This measure is useful only once the kayak is at its fully developed flow speed. The standard deviation calculated during BSA gives a measure of the variability of the result over successive strokes, which is related to the repeatability of movement between strokes. For WSA a model output (such as speed or net paddle force) is averaged within one stroke which gives an average measure that can be used for comparison between different strokes (such as to assess the acceleration of the kayak to its fully developed flow speed). The standard deviation calculated during WSA gives a measure of the variability of the result during each stroke cycle which is related to the efficiency of movement because it quantifies the net reduction in speed due to drag and the net acceleration due to propulsion by the paddle.

3. Verification and validation of the model

The accuracy of fluid-object force predictions has been established for SPH in general (and for the SPH code specifically used here) by Cummins et al. (2012). However such test cases have not specifically addressed the fluid dynamics around a moving hull or a moving paddle. The first test case evaluates the ability of the SPH solver to accurately determine the drag on a streamlined body whilst the following test is for drag on a moving bluff body.

3.1. Validation of fluid dynamics calculations for a moving hull

The accuracy of the fluid simulation around the hull is evaluated here by comparison with experimental measurements of kayaks moving at constant speed (Banks, Phillips, Turnock, Hudson, & Taunton, 2014; Gomes, Ramos, Conceição, Vilas-Boas, & Vaz, 2012; Jackson, 1995; Tzabiras et al., 2010).

Fig. 3 shows the model configuration used for this test case. The hull is the same as for the full athlete-kayak model (Fig. 1) and the tank of water is 3.0 m wide, 1.0 m deep and 40.0 m long. The kayak is settled in the water in an initial simulation step and then the kayak is prescribed to move forwards at a constant speed with all other degrees of freedom fixed. Total force on the kayak is calculated at each timestep using Eq. (6).

Fig. 4 shows the mean drag force for four values of forwards speed and the measured data from four studies by others (Banks et al., 2014; Gomes et al., 2012; Jackson, 1995; Tzabiras et al., 2010). The measured drag force differs somewhat between the experimental studies by up to 30 N, presumably due to variations in athlete mass, measurement techniques, depth of the kayak in the water, and hull design. The simulated results are within 7 N of the experimental results at each speed, which is smaller than the range in experimental results. This comparison indicates that the force results are sufficiently close to measured results for the model results to be considered accurate.

3.2. Validation of fluid dynamics calculations for the paddle blade-water interaction

Next we validate the SPH solver for modelling blade-water interaction during paddling. Sumner, Sprigings, Bugg, and Heseltine (2003) calculated drag coefficients for paddle blades of different design. Using a simulation of the experiments performed by Sumner

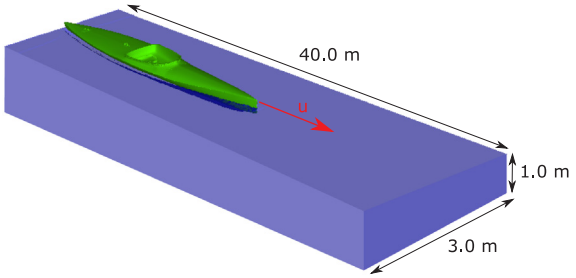

Fig. 3. Simulation set up for the first of three validation and numerical convergence tests. The kayak is placed in a stagnant tank of water 3.0 m wide, 1.0 m deep and 40.0 m long. The kayak moves with a prescribed constant forwards speed (u). The resulting drag force is calculated for comparison.

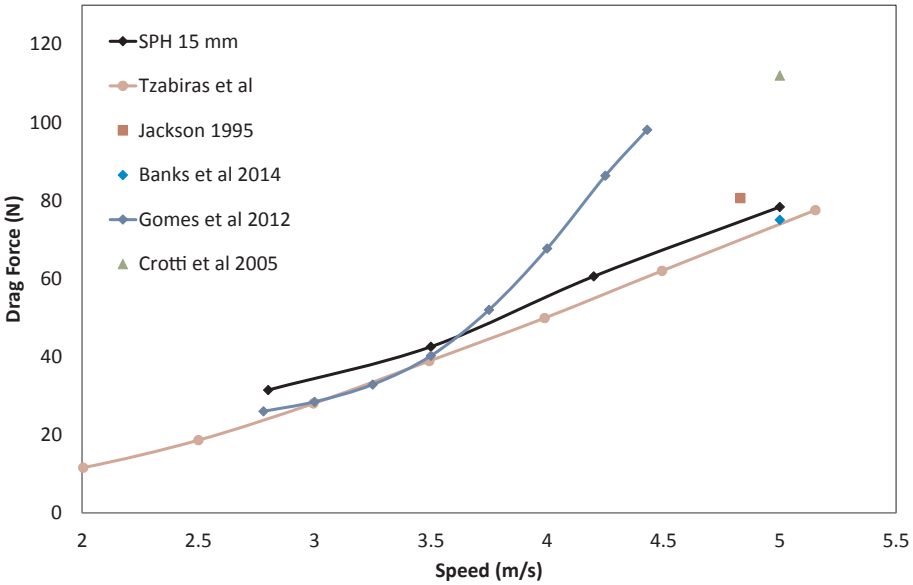

Fig. 4. Drag force on a kayak moving at constant speed as measured in five published studies compared to the calculated drag force for the B-SPH model. Force is expressed in the world reference frame (RF1 in Fig. 1).

et al., we evaluate the accuracy of drag force predictions on the kayak blade for the SPH model.

Fig. 5 shows the model configuration used in paddle-water interaction simulation. The paddle was orientated vertically in a 2.0 m × 2.0 m × 1.0 m tank of stagnant water and only the blade was submersed in the water. The viscosity was that of water (0.001 Pa s) and the SPH particle separation was 15 mm. The blade was prescribed to move at a constant horizontal speed of 1.5 m/s giving a Re = 240,000. The resulting drag force on the blade was calculated for comparison.

The second row of Table shows the resulting drag force calculated for the simulation with the base case SPH particle separation of 15 mm. The calculated drag coefficient of 1.75 is within 1% of the experimental values reported by Sumner et al. This indicates that the model predictions of total force on the paddle blade is sufficiently accurate.

3.3. Numerical convergence with resolution

Numerical convergence has previously been tested for SPH for a range of fluid applications. Cummins et al. (2012) examined convergence for the impact of a sloshing wave on a column structure finding good agreement with experiment with the level of agreement improving with resolutions. Similar results have been shown for other applications of SPH such as the prediction of the energy spectra during turbulence (Di Mascio, Antuono, Colagrossi, & Marrone, 2017), the water entry of solid objects (Kiara, Paredes,

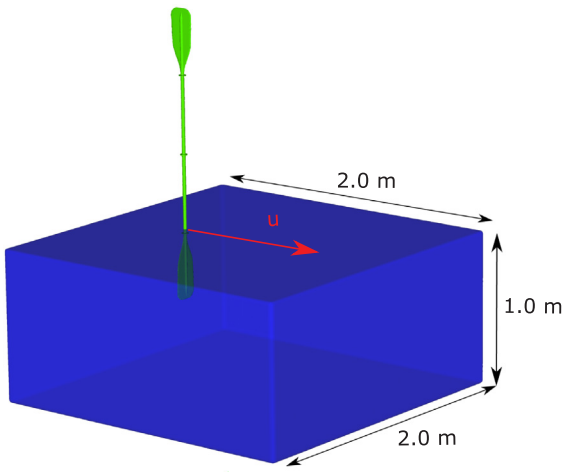

Fig. 5. Simulation set up for the second of two validation and numerical convergence tests. The paddle is placed in a stagnant tank of water 2.0 m wide, 1.0 m deep and 2.0 m long. The paddle is prescribed to move forwards at a constant speed (u) and the resulting drag force is calculated.

Table 2
Calculated drag force on a kayak paddle pulled through a tank a water compared to the experimental results of Sumner et al. (2003).

Particle separation (mm)	Number of particles	Mean drag force on the paddle blade (N)	Successive difference (%)	Measured drag force (N) (Sumner et al., 2003)
20	0.5 M	118	–	102–105
15	14 M	110	+14	
12.5	23 M	107	+4	

& Yue, 2017) and ice shelf dynamics (Pan, Tartakovsky, & Monaghan, 2012).

Whilst these studies of resolution dependence provide a general level of reassurance of solution accuracy, the current problem is very complex with several components which are beyond what has been tested in these earlier studies. We therefore evaluate the sensitivity of

1. the drag force on the hull (introduced in Section 3.1);
2. the drag force on the paddle blade (introduced in Section 3.2); and
3. the drag force on the paddle blade for the complete dynamic model (as described in Section 2)

on the spatial SPH resolution used.

The particle sizes used in this convergence study are listed in the first columns of Tables 2–4. The criterion chosen for acceptability of the solution was that the difference in drag force between two resolution cases was less than 5%, which is sufficient for the purposes of understanding the kayak dynamics. The results for Case 1 are shown in Table 3. The difference between results for resolutions of 20 mm and 15 mm is 1%, demonstrating that the 15 mm resolution is well converged and very accurate for this application. The mean values of drag force for Case 2 are given in Table 2. The force is shown to both converge and have less than a 5% difference between the 15 mm and 12.5 mm resolution cases. The mean drag force on the paddle blade in Case 3 for the first stroke is given in Table 4. Since the mean drag for the 15 mm resolution case is within 5% of the 12.5 mm resolution case, we conclude that a resolution of 15 mm is sufficient to well resolve the flow for the purposes of this study.

Table 5 lists the mean drag force on the hull for three variants of water tank dimensions. The results show that the results for the base case (3 m wide and 1 deep) are not significantly changed when a wider (4 m) or shallower (0.85 m) tank is used. This indicates that the simulation predictions are sufficiently independent of tank depth and width.

4. Dynamics of the kayak acceleration to equilibrium speed

At the start of a kayak race there is a quick acceleration to equilibrium speed and it is not yet known quantitatively how variations to paddle and kayak design or changes to stoke technique affect the rate of acceleration. Here we investigate the relationship between fluid dynamics, paddle and kayak motions, and fluid forces for six strokes during the acceleration to equilibrium speed for the 135SPM case.

The motions of the athlete, paddle, kayak and fluid free-surface behaviour, as well as the fluid surface speeds are shown in Fig. 6 for the first two strokes at 135 spm. All motions are calculated in the world reference frame (RF1 in Fig. 1). At the start of the second cycle (1.20 s), a bow wave has formed and the fluid within it is moving at moderate speed (0.3 m/s). The water in the wake of the kayak is also moving at approximately 0.3 m/s. The fluid near to the hull is entrained by skin friction drag forces, with speed tending to the hull speed with increasing proximity to it. The left hand is the thrust hand or this stroke and pulls the paddle blade towards the stern whilst the right (draw) hand pushes towards the bow. As the blade enters the water for the left side stroke (shown first) the fluid speed near to the blade quickly exceeds 0.7 m/s and significant displacement occurs. At the end of the pull phase of the left stroke (1.30 s), the water that has interacted with the paddle has been energetically displaced, resulting in splashing. This surface disturbance on the left has begun to dissipate at the beginning of the right side stroke (1.67 s). During the right side stroke (1.67–1.77 s) the right hand is now the thrust hand and the left hand is the draw hand. Fluid behaviour during the second left side catch (1.67 s) and pull (1.77 s) phases is similar to that of the first left side stroke. During the first two strokes the within stroke averaged (WSA) forwards speed of the kayak increases by 0.3%.

During the third stroke (2.07–2.17 s) the WSA forwards speed increases by 0.1% and consequently the peak fluid speed in the bow wave has also increased to more than 0.4 m/s. The extent of disturbance to the fluid surface due to the left side stroke (from 2.07 to 2.17 s) is less than for the previous stroke (which was from 1.20 s to 1.30 s). This occurs because the kayak is now moving at closer to its equilibrium speed, so the blade-water velocity difference is lower and the force imparted to the water is smaller. Similarly, the

Table 3
Dependence of drag force on SPH resolution for the test case of a hull moving through water at a constant speed.

Particle separation (mm)	Number of particles	Mean drag force on the kayak hull (N)	Successive difference (%)
20	15 M	67.0	–
15	37 M	67.7	1.0

Table 4
Dependence of drag force for the paddle blade on SPH particle resolution for the B-SPH kayak model.

Particle separation (mm)	Number of particles	Peak force on paddle blade (N)	Successive difference (%)
20	15 M	153	–
15	37 M	260	41%
12.5	62 M	250	4%

Table 5
Dependence of drag force for a kayak moving through water at a constant speed on width and depth of the water tank.

Case	Width (m)	Depth (m)	Mean drag force on kayak (N)	Difference from base case (%)
Base case	3.0	1.0	67.7	–
Increased width	4.0	1.0	66.7	1.4%
Decreased depth	3.0	0.85	66.9	1.2%

water velocities during the next right side stroke (2.57–2.63 s) are smaller than for the previous stroke and the surface disturbance is again smaller. Whilst the simulated kayak is able to move both vertically and horizontally, as well as to pitch, roll and yaw, the stroke technique is sufficiently realistic so the model kayaker is able to maintain balance and to generate motion that is dominantly in the forwards direction. If the force and torque balances on the kayak favoured tipping over then this model is able to predict such behaviour. The stability of the predicted motion is a consequence of force balances within the model that lead to stable kayak orientation.

The passage of the blade and the kayak through the water generates three dimensional flow around them which includes vortical structures. These can be visualised by rendering isosurfaces of constant vorticity (identified using the λ_2 method, see Section 2.4) as shown in Fig. 7 at three times during the third stroke for 135 SPM. As the kayak hull moves forwards, it separates water at the bow and accelerates it into the bow wave. Vortices are shed from the front of the kayak as the bow wave surges forward. They travel down the length of the hull and become less coherent after they pass the mid-length of the kayak. Strong vortices are created when the flow separates from the keel and these interact with vortices formed in the stern wake. Fig. 7a shows a large vortex forming as the paddle enters the water. After the paddle is removed from the water at the end of the stroke (Fig. 7b), this structure has grown in size, primarily by elongation in the forward-rear direction. As the athlete prepares for the fourth stroke (0.2 s later, see Fig. 7c), this vortical structure is still present, but has moved backwards relative to the kayak. The large size and long lifespan of these coherent structures indicate that a significant amount of energy has been transferred from the blade to the water, as the stroke accelerates the kayak forwards. In fact the large size of the vortices indicates the substantial amount of the propulsion generated by a single stroke (Michael et al., 2009). At equilibrium speed the blade-water interaction forces are smaller which results in smaller vortex structures.

Fig. 8 shows the predicted components of linear speed and orientation of the kayak with increasing numbers of strokes for the 135SPMAcc case. The forward speed (Fig. 8a) is 4.6 m/s the start of the first stroke cycle and increases sharply once the blade enters the water. The water is initially moving slowly relative to the blade, so large propulsive forces are generated by the paddle as it is pulled through the water. The force generated by the moving paddle is larger than drag on the hull and so the forward speed of the kayak (Fig. 8a) increases rapidly. Between strokes the forward speed decreases modestly due to short term dominance of the hull drag. As the speed of the kayak increases with each stroke, the relative speed between the blade and the water decreases and so the propulsive force generated by the blade-water interaction progressively decreases. When the kayak is moving sufficiently fast, the propulsive force reaches equilibrium with the drag force and no further net acceleration occurs so the peak forward speed remains constant for further strokes. A statistically stationary state was achieved within the five of the six strokes simulated.

The sideways and vertical components of linear speed and orientation angles of the kayak show cyclic variations with a period equal to the stroke rate which are all caused by the combination of the interaction of the paddle with the water and the movement of the athlete's centre of mass throughout the stroke (Fig. 8b–f). When the blade enters the water this generates a force onto the blade which is predominantly oriented in the forwards and upwards direction. This force creates a torque about yaw, roll and pitch axes. With each stroke the athlete reaches to one side, shifting their centre of mass from the centreline of the boat to the stroke side, causing the kayak to roll. For most of the degrees of freedom the average position or angle is approximately zero but a gradual drift is observed for the roll. This drift will eventually result in capsizing if not corrected by the athlete. The roll (Fig. 8b) oscillates between 0.5° and 1.0° during the first few strokes as a result of the periodic movement of the centre of mass of the kayak-blade-athlete shifts resulting from the kayaker leaning into each stroke. The vertical speed (Fig. 8c) is small (less than 0.05 m/s) and oscillates between 0.0 m/s and 0.05 m/s with each stroke. When the blade enters the water the water creates a buoyancy force onto the blade, which lifts the kayak slightly. As the paddle is removed from the water the kayak settles back into the water under gravity.

Prediction of the loading on the paddle and throughout the athlete's body allows for detailed assessment and enhanced understanding of athlete technique. Quantitative information provided by the model can be used to evaluate proposed technique changes and equipment modifications without impacting on the training regime of an athlete or building expensive prototypes. The force on the paddle is determined by the relative speed between the paddle and the water and the orientation of the paddle to the water surface (which is a function of kayak and body orientations) as it enters the water. The force is zero when the paddle is out of the water and rises sharply immediately after water entry. The force on the paddle is then a function of surface area and the relative

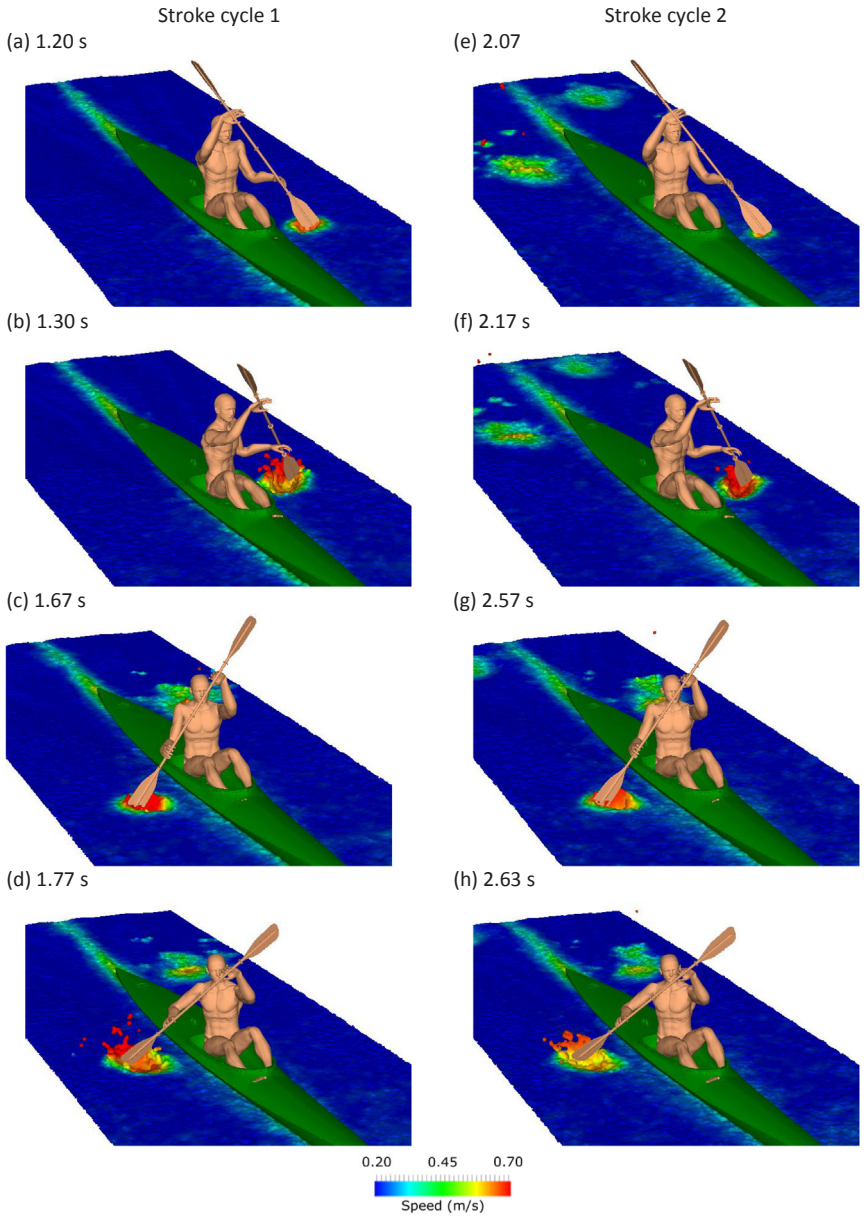

Fig. 6. Motion of the athlete, paddle, kayak and water surface at different times during two successive stroke cycles of the 135 SPM case. The water is coloured by its speed and the timing of the image is shown in seconds. Speed is expressed in the world reference frame (RF1 in Fig. 1).

speed to the fluid with which it is interacting.

The area of the paddle underneath the water surface and the magnitude of the resulting force on the paddle blade for the first six strokes are shown in Fig. 9. During the first three strokes the roll is negligible and therefore the area of the paddle underneath the water surface is approximately constant. As a consequence of this and since the kayak is accelerating modestly (reducing the relative speed of paddle to water) the paddle force decreases steadily in magnitude. During the fourth to sixth strokes the kayak begins to roll to the left which leads to substantial asymmetries in the submerged paddle area and the resulting paddle force. The roll angle at the start of the second right hand side (RHS) stroke is 0.72° less than for the start of the first RHS stroke causing the submerged area of the right paddle during the second RHS stroke to be 11% less than for the first. As a result the peak force during the second RHS stroke (191 N) is substantially less than for the first RHS stroke (246 N). During the third left hand side (LHS) stroke the submerged area of the paddle is 28% larger than for the second LHS stroke and thus the opposite effect occurs: the peak paddle force is 274 N during the third LHS stroke is larger than for the second (244 N). With pre-defined kinematics the resulting dynamical behaviour of the system can be stable (where the roll does not grow unboundedly) or unstable (where the roll increases to an extent that will lead to the kayak capsizing). This highlights the adaptive role of the athlete in maintaining the balance of the kayak-kayaker system. Since the athlete

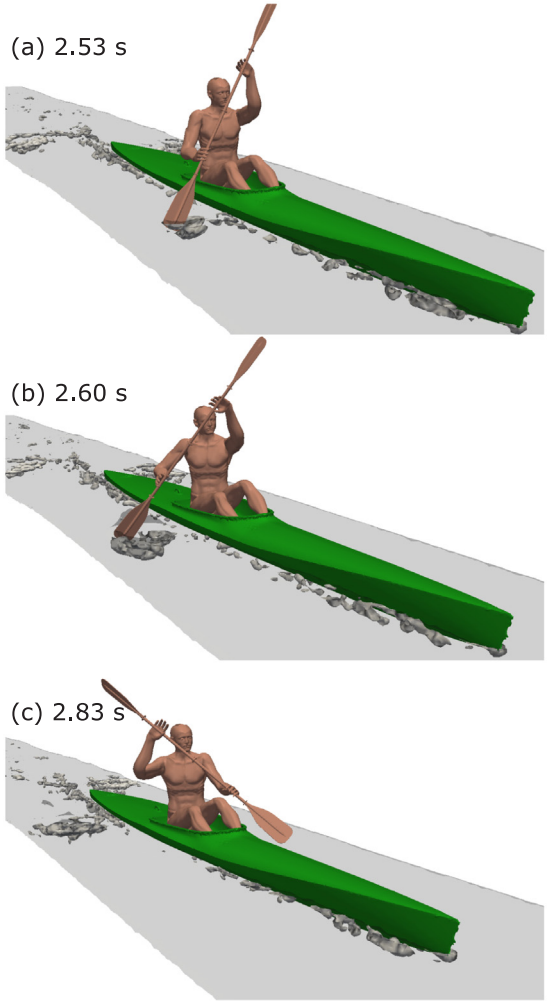

Fig. 7. 3D vortex structures shed from the front and rear of the kayak and from the interaction of the blade and water for, the (a) blade catch, (b) blade release and (c) as the athlete prepares for the next (left side) stroke.

cannot perform perfectly symmetric kinematics (which are expected to be optimal from an efficiency perspective) while maintaining the balance of the kayak. Instead the kayaker performs micro adjustments to their body pose and their stroke technique to minimise out-of-balance forces and to maintain stability of their roll angle.

In the next section we focus on the equilibrium phase of racing in which symmetric stroke technique (without dynamic adjustment) is sufficient for maintaining balance of the kayak for a more substantial period of time.

5. Effect of stroke rate on equilibrium kayak speed and paddle forces

After the early part of a race when the athlete accelerates the kayak from a stationary position, and before substantial fatiguing occurs, there is a period of time in which the stroke technique and peak paddle forces remain approximately constant. Here we use the term “equilibrium speed” to designate this period when the peak speed and force during each successive stroke cycles is approximately invariant. Peak paddle force is defined as the maximum force on the paddle for a particular stroke cycle. In this section we investigate the relationship between stroke rate and the resulting equilibrium performance (in terms of speed and peak paddle forces generated by the athlete).

Fig. 10 shows the forward speed and paddle force in the world coordinate frame (RF1 In Fig. 1), between stroke averaged (BSA) over the first four stroke cycles for the three stroke rates cases − 135SPM, 115SPM and 95SPM. One standard deviation in forward speed and paddle force is also shown as thin lines above and below the average curves. Standard deviation between strokes indicates the variation in the results between stroke cycles. In Fig. 10 the standard deviations are consistently small throughout the stroke for each of stroke rates. The lack of variation in the speed and force results between strokes confirms that the kayak and athlete are operating at equilibrium conditions. It also indicates that the stroke and the resulting system dynamics has a high degree of

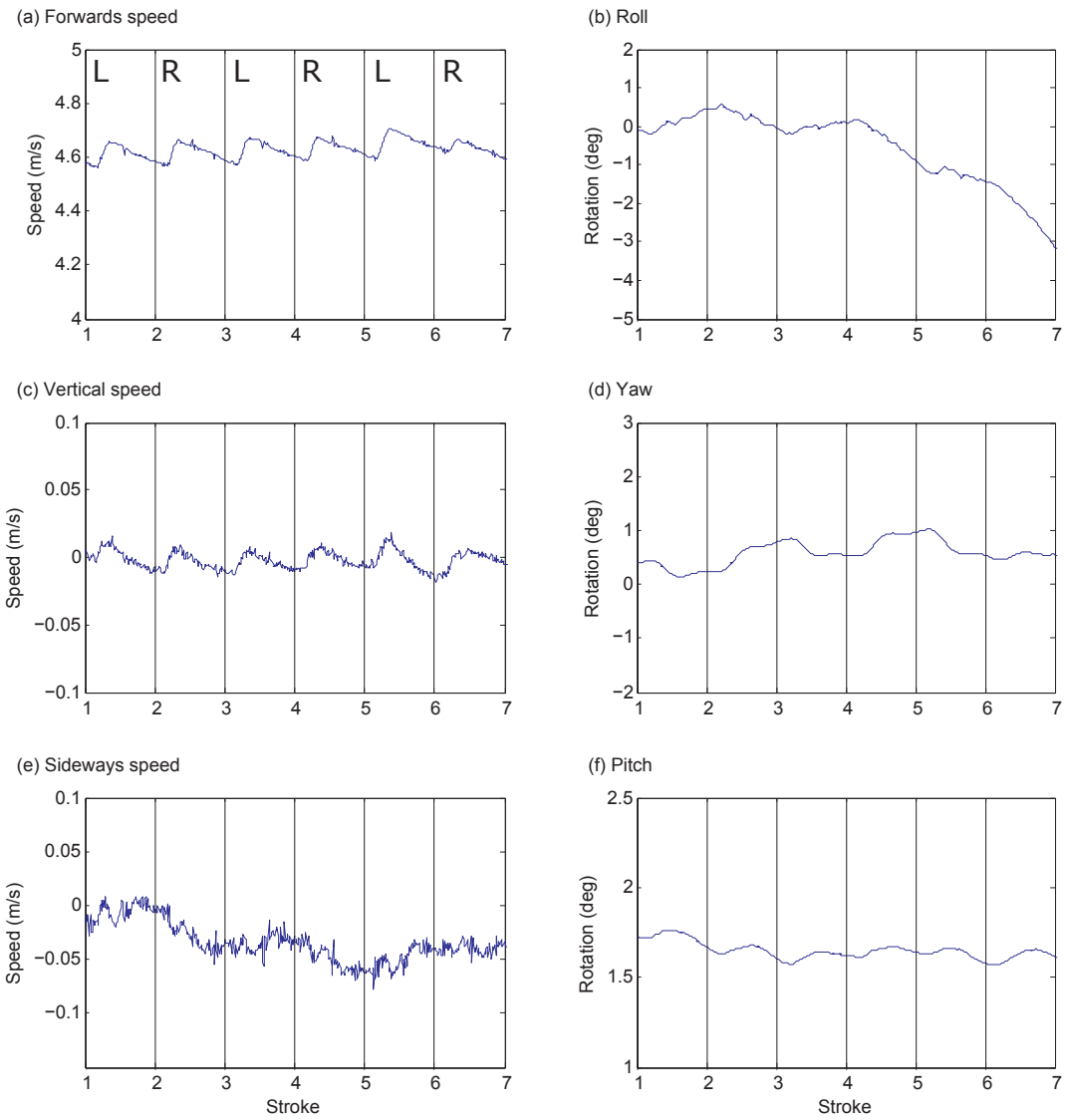

Fig. 8. (a) forward speed, (b) roll, (c) vertical speed, (d) yaw, (e) sideways speed and (f) pitch of the kayak versus stroke number over eight stroke cycles, for 135 spm. Movements are expressed in the world reference frame (RF1 in Fig. 1). The black vertical lines indicate the start of each stroke with the L and R in (a) indicating whether the paddle interaction with the water is on the left or the right side of the kayak.

reproducibility between strokes. Both speed and force increase with increasing stroke rate because the paddle is moving faster relative to the kayak.

Table 6 gives the between stroke averaged (BSA) forward speed of kayak and peak paddle forces in RF 1 over the four stroke cycles at equilibrium speed. The forward speed increases approximately linearly with increasing stroke rate. In contrast, the magnitude of peak paddle force increases logarithmically with stroke rate. The predicted WSA forward speed of 4.68 ± 0.01 m/s for the 135 SPM case is consistent with the peak racing speed of elite athletes (Baker et al., 1999). The predicted peak force of 211 ± 13 N at a speed of 4.68 m/s is close to the measurements of Gomes et al., 2015 (which was 266 ± 33 N) at a speed of 4.58 ± 0.20 m/s, especially when considering the differences in paddle design and stroke kinematics used. These comparisons of predicted speed and force with previously reported experiments are favourable and give confidence in the reasonableness of the model outputs.

Whilst paddle force is a reasonable indicator of the load on the body, it is more useful to calculate the actual loading on each hand throughout the stroke cycle as this more precisely quantifies the differential body loading between the simulation cases. Fig. 11 shows the left and right hand forces during each stoke as averaged across the first four stroke cycles. During the first (left hand dominated) stroke the draw hand is the right and the thrust hand is the left. The force on the thrust hand, as shown in Fig. 11c, is larger than the force on the draw hand (Fig. 11e), by approximately 51% for each case. This larger force at the hand results in a substantially larger torque about the torso. The athlete necessarily needs to generate large forces in their lower back and legs to counteract the torque generated by the left and right hand forces on the paddle. During the second (right) stroke the right (thrust) hand force (shown in

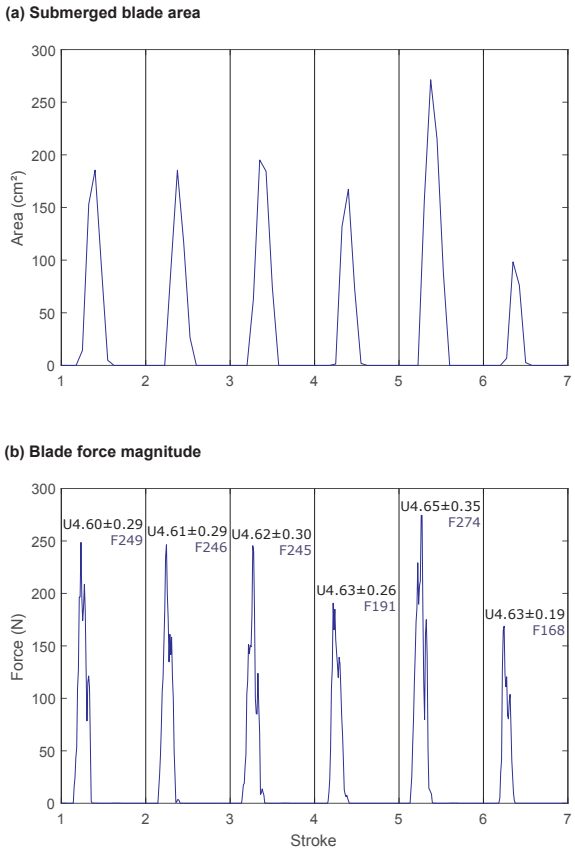

Fig. 9. (a) Total submerged area of the paddle and (b) total force on the paddle blade vs. stroke cycle for the 135 SPM case. Force is expressed in the world reference frame (RF1 in Fig. 1). In (b) the speed of the kayak in each stroke cycle is indicated with a "U" followed by the mean speed ± standard deviation in m/s. The peak force on the paddle is indicated with an "F" followed by the peak paddle force in Newtons.

Fig. 11f) is larger than the left (draw) hand (by approximately 53% for each case). These ratios of force between the left and right hands for the first and second strokes are approximately equal because they are a function of the moment arm of the force on the paddle blade about the hands (which does not vary with time). The large magnitudes of hand force for each of the three stroke rates indicates a need for substantial strength in the arms, and the endurance to maintain these forces throughout a race.

6. Analysis of stroke asymmetry

It is known that elite athletes use a more symmetric stroke than do amateur athletes (Helmer et al., 2011; Limonta et al., 2010). Also, it is usually expected that stroke symmetry is related to energy efficiency, but the differences in kayak speed and the loading on the body that result from changes to stroke symmetry have not been quantified or analysed.

The predicted linear speed and orientation of the kayak are shown for the simulation cases 135SPMAcc, Asymm1 and Asymm2 in Fig. 12 and the corresponding submerged paddle area and paddle forces are shown in Fig. 13. All motions and forces are calculated in the world reference frame (RF1 in Fig. 1). In each case the forward speed of the kayak (Fig. 12a) increases with each stroke (as was explored in Section 4). As asymmetry is increased the depth of the right side paddle stroke relative to the kayak hull decreases but the left side paddle stoke remains unchanged. The decreased depth of paddle stoke on the right side reduces the submerged surface area of the paddle which therefore decreases the drag force generated on this side. As a result the speed increments added to the kayak during the strokes by the right hand are progressively smaller with increasing asymmetry. After the first full stroke cycle, the speed of the kayak is 4.59 m/s for the symmetric case, 4.56 m/s for the Asymm1 case and 4.52 m/s for the Asymm2 case. These represent 0.7% and 0.9% decreases in speed respectively, which are significant at the elite level of competition. The roll angle of the kayak (Fig. 12b) diverges after the first RHS stroke (stroke 2) in response to the different depths of paddle stroke. At the start of the third stroke there is 0.55° difference in roll angle but by the start of the fifth stroke the difference in roll angle between the three simulation cases has increased to 2.5°.

The differences in prescribed stroke technique and identified variations in orientation and speed of the kayak cause substantial differences in the area of the paddle that is submerged and therefore in the paddle force (Fig. 13). For the Asymm1 case the first RHS stroke has 35% lower submerged paddle area which results in a proportional 34% reduction in paddle force. The Asymm2 case has 69% lower submerged paddle area and a 47% reduction in force. Despite the left hand kinematics being the same for each of these

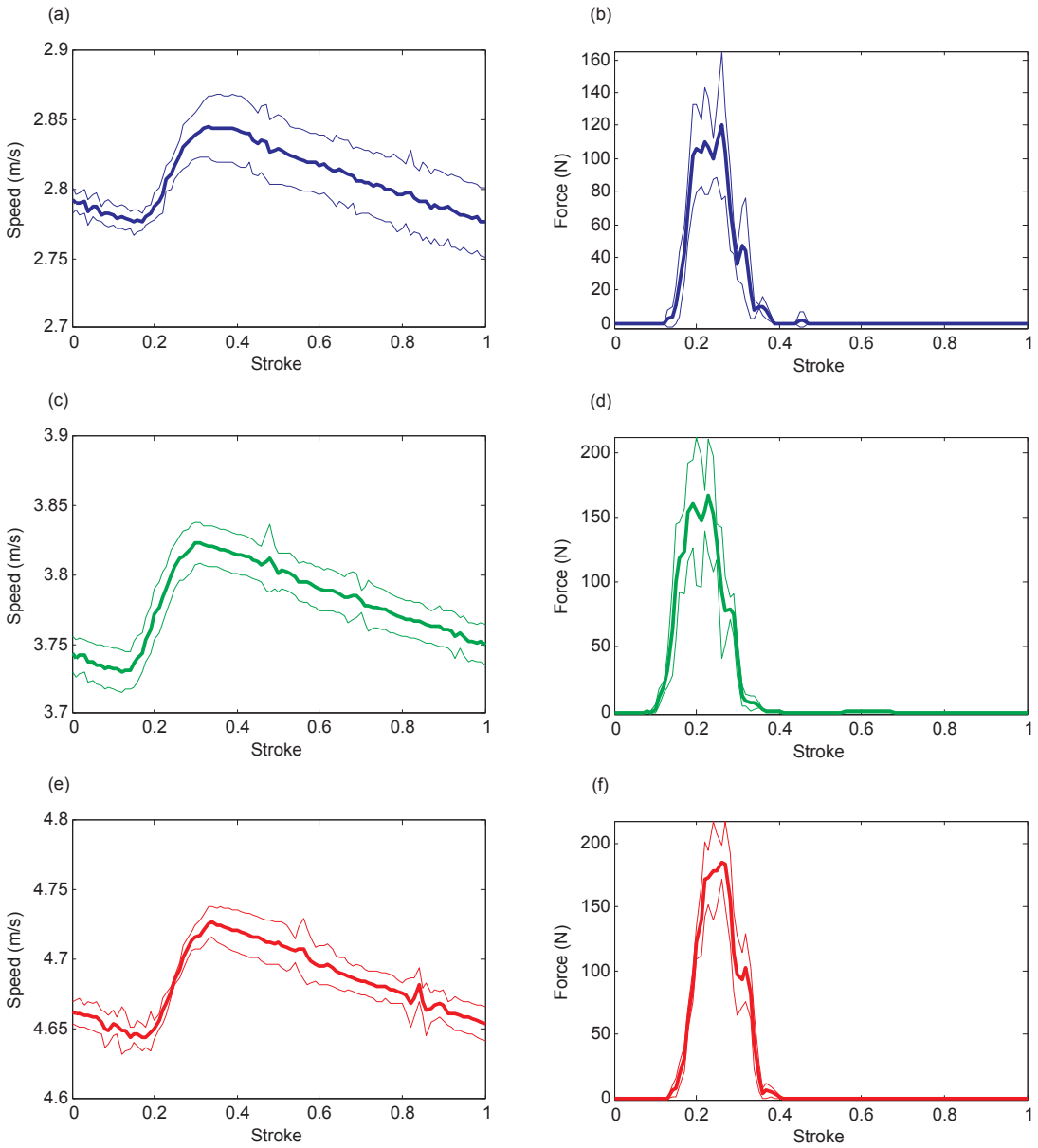

Fig. 10. Between stroke averaged (BWA) forward speed (left panels) and net paddle force (right panels) vs. stroke phase for the first four strokes (two left and two right strokes) at 95 spm (top row), 115 spm (middle row) and 135 spm (bottom row). Force and speed are expressed in the world reference frame (RF1 in Fig. 1). One standard deviation from the BWA forwards speed and paddle force is shown by the thin lines above and below the averaged curves.

Table 6
Forward speed of kayak and peak paddle force for a kayak at equilibrium for the three simulated stroke rates.

Case	Equilibrium Speed (m/s)	Peak force (N)
95SPM	2.81 ± 0.01	144 ± 33
115SPM	3.78 ± 0.01	200 ± 32
135SPM	4.68 ± 0.01	211 ± 13

cases the peak forces on the second left side stroke are not the same for the three simulation cases (Table 7). This is a result of the roll of the kayak to the left side which is generated by the asymmetries in the first right hand stroke (Fig. 12b) which then causes the submerged area for the left side stroke to decrease (by 10% for Asymm1 and 18% for Asymm2) which in turn reduces paddle force

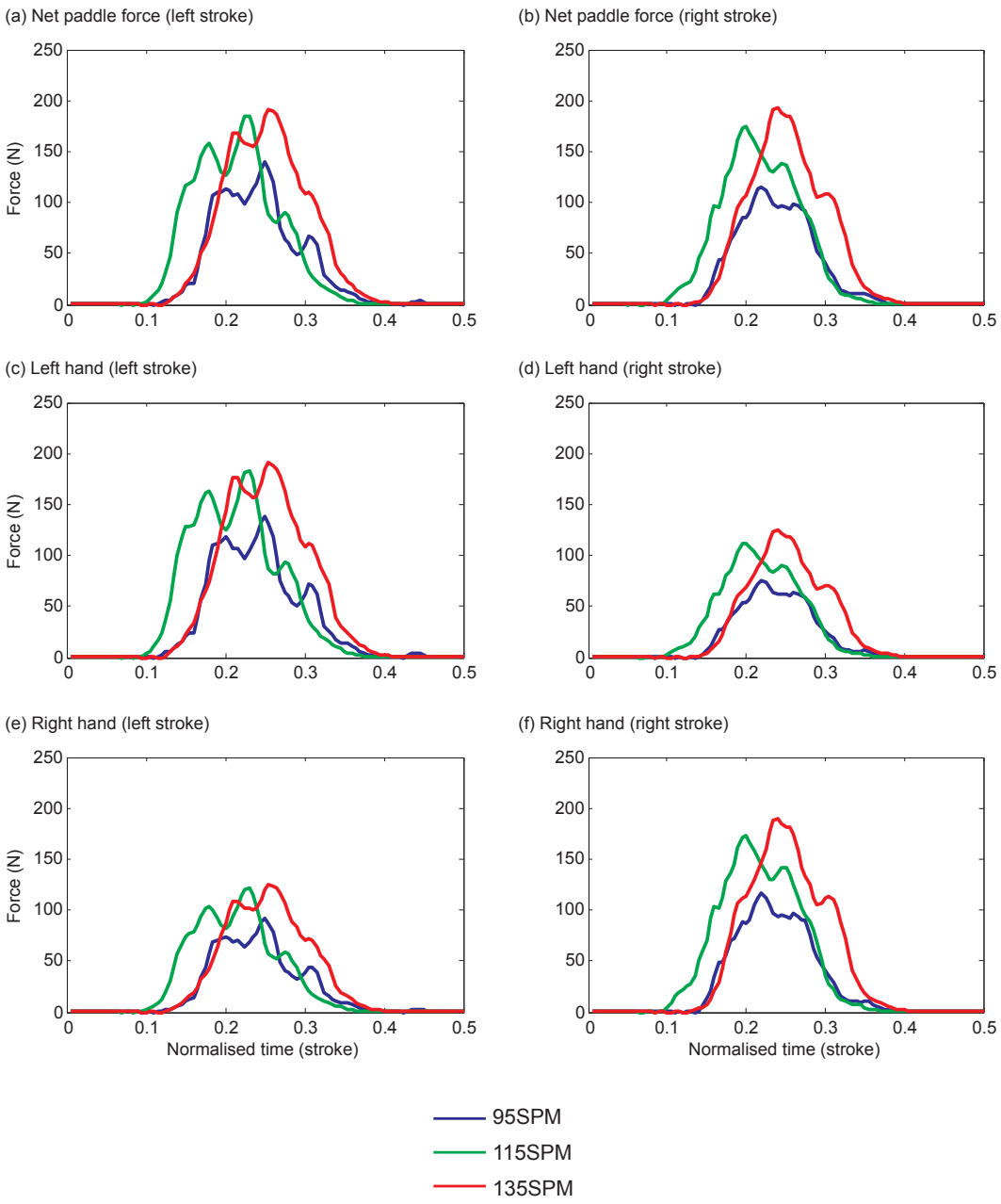

Fig. 11. Magnitude of force on (a and b) the paddle, (c and d) left hand, and (e and f) right hand during the fifth (shown on the left) and sixth (right) strokes for three simulated stroke rates. Force is expressed in the world reference frame (RF1 in Fig. 1).

(Fig. 13a). Conversely, the speed of the kayak is slower with increased asymmetry (Fig. 12a) which increases paddle force because of the larger speed differential between paddle and water. For the Asymm1 case this increase in speed differential counteracts the effects of reduced submerged area and together they cause the LHS force to be 5% larger than for the symmetric case. For the Asymm2 the effects of reduced submerged area are sufficiently large to cause the LHS force to be 29% larger than for the symmetric case (135SPMAcc). After four strokes the Asymm1 case is travelling 1% slower than the symmetric case and the Asymm2 case is travelling 3% slower than the symmetric case.

The effects of asymmetry of stroke style (and the resulting asymmetric motion of the kayak) on body loading are even more apparent in the calculated force on each hand (Fig. 14). The peak force on the left hand during the left stroke (Fig. 14c) is approximately the same as for the right hand during the right stroke (Fig. 14f) for the symmetric stroke. However, when asymmetry is present this is no longer the case. The peak left hand force is 45% larger than the peak right hand force during the right side stroke for the Asymm1 case and 143% larger for the Asymm2 case. This means that there is a clear penalty for having an asymmetric stroke

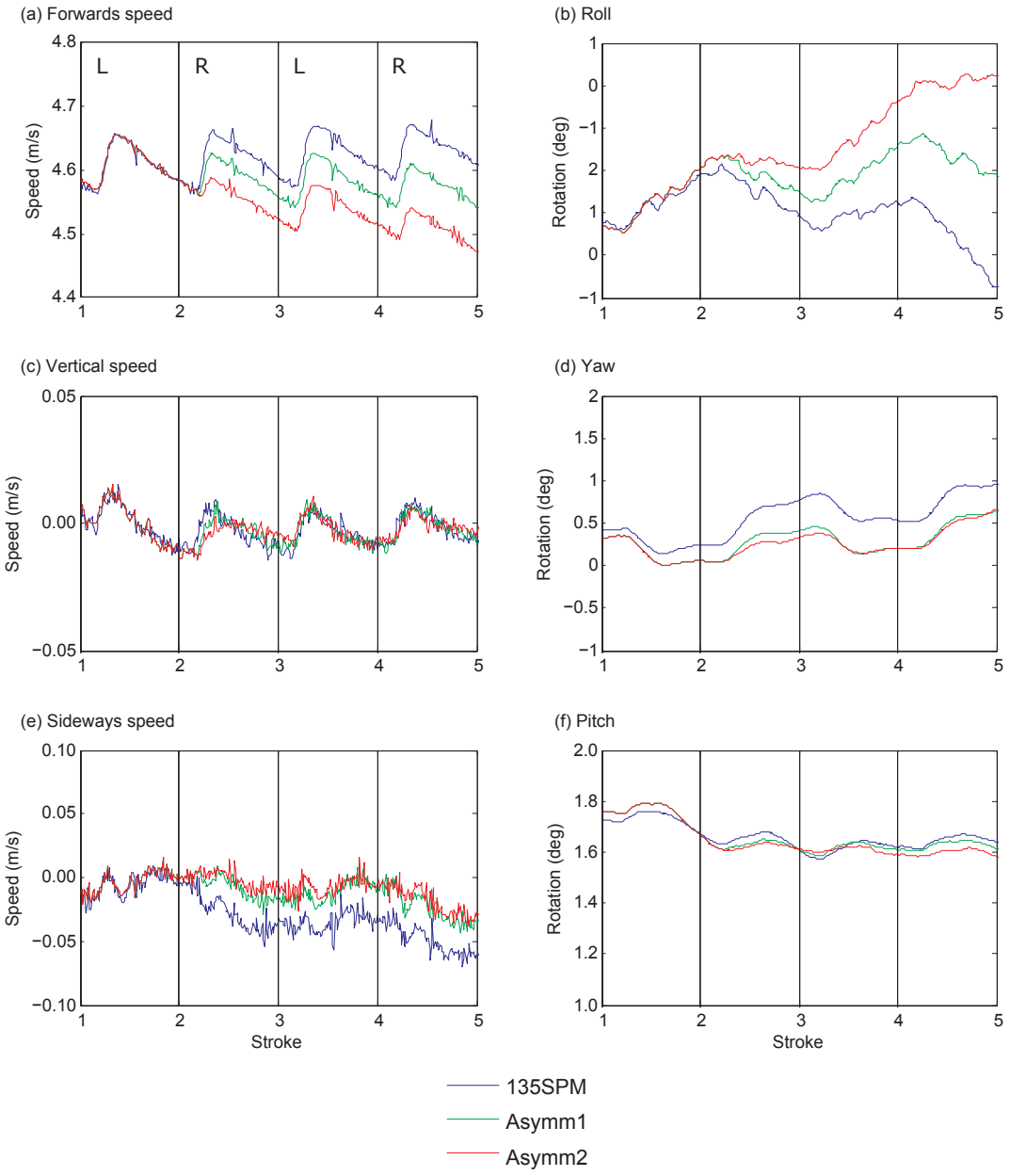

Fig. 12. (a) forward speed, (b) roll, (c) vertical speed, (d) yaw, (e) sideways speed and (f) pitch of the kayak versus stroke number over four stroke cycles, for three simulated variants with differing stroke symmetry. Movements are expressed in the world reference frame (RF1 in Fig. 1). Left side strokes are labelled "L" and right side strokes are labelled "R". Start and end of strokes are denoted by the vertical lines.

which is partially manifested as a slower average speed but also by imbalances in the forces on the body. These will generate unbalanced muscle forces which are much larger for the left side of the body and which will have significant implications for fatigue and left-right asymmetry in muscle growth.

7. Future work and extensions of the current model

The model presented is sufficiently general that many applications can be investigated to understand how technique, strength, endurance and equipment design affects racing speed. Individual stroke technique of elite athletes can be input from 3D motion capture. The causes of performance differences between athletes will be studied in greater detail than physical measurements allow. Studies of starting, steady state and fatigued racing technique will be performed for a range of individuals and equipment choices (kayak and/or paddle variants). These simulations will be able to provide quantitative evidence for evaluating the benefits or

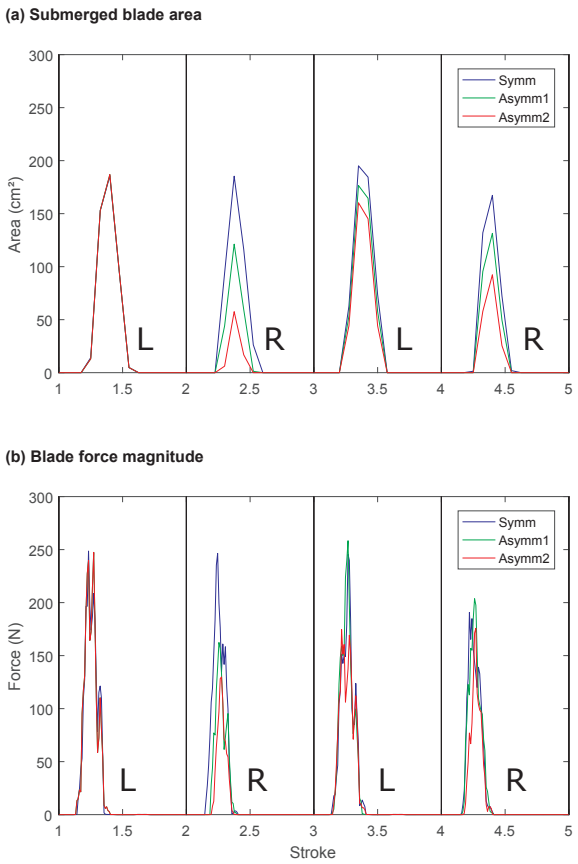

Fig. 13. (a) Total submerged area of the paddle and (b) total paddle force versus stroke phase over four stroke cycles, for three simulated variants with differing stroke symmetry. Left side strokes are labelled "L" and right side strokes are labelled "R". Start and end of strokes are denoted by the vertical lines. Force is expressed in the world reference frame (RF1 in Fig. 1).

Table 7
Equilibrium forward speed and the peak paddle force during the first four strokes for cases with decreasing stroke symmetry at 135 SPM.

Case	Speed (m/s)	Peak force (N)	
		Left	Right
135SPMAcc	4.63 ± 0.03	247 ± 2	219 ± 39
Asymm1	4.57 ± 0.02	253 ± 8	183 ± 29
Asymm2	4.51 ± 0.02	211 ± 51	153 ± 32

disadvantages of specific coaching decisions. Hypothetical changes to technique, strength and equipment will be able to be assessed in future work for individual athletes to optimise performance. These data-rich model results provide information that cannot be measured in physical experiment such as individual hand forces.

Future extensions of the biomechanical component of the current model such as calculations of joint torques and joint power (Harrison et al., 2016) will enable feedback of the load onto the athlete kinematics to be included as well as facilitating calculation of energy utilisation for different stroke techniques and equipment designs. Weaker fluid dynamical effects such as that of air entrapment (which can be modelled by using two sets of SPH particles to represent the water and gas phases) and its break-up into bubbly flow behind the blade (using coupled discrete bubble models, such as described in Cleary, Pyo, Prakash, & Koo, 2007b). Aerodynamic load on the kayaker and the kayak, such as when strong cross winds are present, can also be included as drag loads on the biomechanical structure. Whilst individually small in their effects, these should eventually be included in a comprehensive model.

8. Conclusions

In this paper, we have presented a dynamic, 3D, coupled biomechanical-SPH modelling for predicting performance in kayak

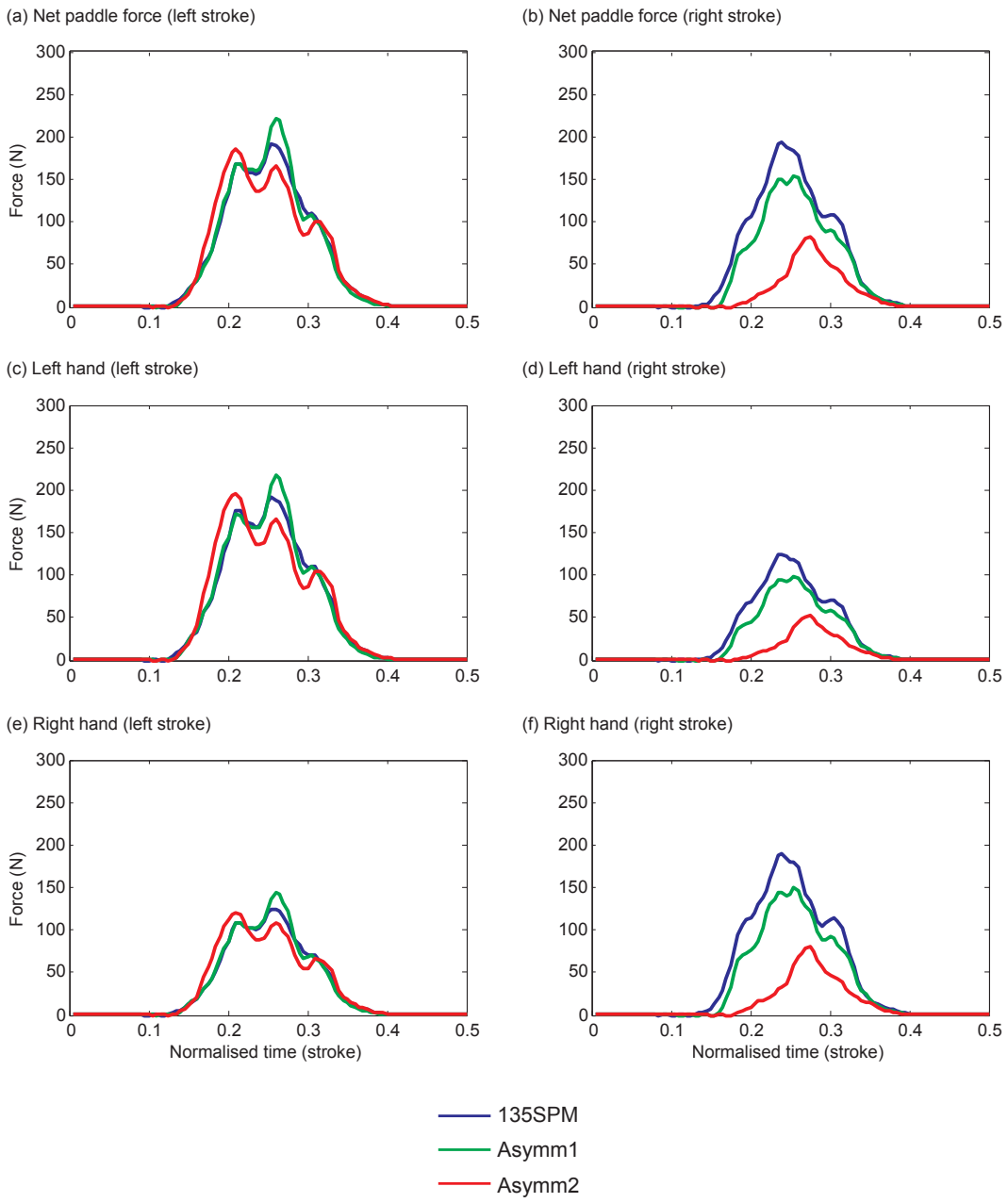

Fig. 14. Magnitude of force on (a and b) the paddle, (c and d) left hand, and (e and f) right hand during the third (shown on the left) and fourth (right) strokes for three simulated variations with differing stroke symmetry. Force is expressed in the world reference frame (RF1 in Fig. 1).

racing. The framework introduces a number of aspects that have not been modelled in other studies, including

1. Biomechanical representation of the athlete (skeletal kinematics) coupled to the paddle, kayak and to a fluid dynamics solution.
2. Free surface fluid dynamics due to kayak motion and blade-water interactions.
3. Fully dynamic (six degrees of freedom) motion of the kayak, athlete and paddle and full coupling between them.
4. Calculations of force on the paddle blade and the hands.

The model predicts the full translation and rotational movements of the kayak through the water. The kayak accelerates quickly during the first few strokes and then reaches an equilibrium speed. All aspects of fluid dynamics are simulated, including the bow wave, the wake, and interactions between paddle and water which cause splashing, fragmentation and the creation of three dimensional vortex structures. Model results are shown to produce valid results and the resolution is shown to be sufficiently accurate

for this application. The racing speed and paddle forces predicted by the model are consistent with published data. Future extensions of the model will include the calculation of joint torques, joint powers and direct prediction of stroke technique for changes to athlete strength and endurance.

The B-SPH kayak model is much more general than statistical measured data based models and therefore can be used to increase understanding of the relationships between performance and stroke technique, strength and endurance, and equipment design, particularly in circumstances that have not been measured. The model can be used to test hypotheses relating to changes to these variables in a controlled manner and provides a much richer set of data than can be measured in physical experiment enabling more informed hypothesis formulation and optimisation choices. The two examples of application of the model described in this paper are the investigation of stroke rate variation and decreases left-right stroke symmetry. They illustrate both the model generality and usefulness of the specific model outputs.

The effect of varied stroke rate and stroke asymmetry on racing speed, fluid dynamics and forces on the paddle and hands was studied using the model.

- The equilibrium forward speed of the kayak increases logarithmically with stroke rate as does the peak blade force. The force on the thrust hand is larger than that for the draw hand and the magnitudes of these forces also increase with stroke rate. Equilibrium speed was achieved after four strokes for the 95 SPM case, but takes longer with increasing stroke rate.
- Increased asymmetry of stroke depth reduces the forwards speed of the kayak and causes a substantial left-right imbalance in forces on the body. As the depth of the right side stroke decreases so too does the speed increment added by the right side stroke. In partial compensation, the speed increment added by the alternating left side stroke increases because the relative speed of the paddle blade to the water is larger. The combined effect leads to the speed decreasing with increased stroke asymmetry because the left side cannot completely compensate for the speed lost on the right hand side without increasing stroke depth. These results suggest that fatigue may occur more quickly on the dominant side (left in this case) when the stroke is sufficiently asymmetric.

Acknowledgements

The authors gratefully acknowledge video footage and technical input from Andrew Eddy, and input from the earlier kayak computational modelling work by David Gunn.

Appendix A. Supplementary material

Supplementary data to this article can be found online at https://doi.org/10.1016/j.humov.2019.02.003.

References

Anderson, F. C., & Pandy, M. G. (1993). Storage and utilization of elastic strain energy during jumping. *Journal of Biomechanics, 26*(12), 1413–1427.
Baker, J., Rath, D., Sanders, R., & Kelly, B. (1999). A three-dimensional analysis of male and female elite sprint kayak paddlers. In ISBS-Conference Proceedings Archive (Vol. 1).
Banks, J., Phillips, A. B., Turnock, S. R., Hudson, D. A., & Taunton, D. J. (2014). Kayak blade–hull interactions: A body force approach for self-propelled simulations. *Proceedings of the IMechE, 228*, 49–60.
Batchelor, G. K. (1973). *An introduction to fluid dynamics.* Cambridge University Press.
Bishop, D. (2000). Physiological predictors of flat-water kayak performance in women. *European Journal of Applied Physiology, 82*(1–2), 91–97.
Buckeridge, E. M., Bull, A. M. J., & McGregor, A. H. (2014). Biomechanical determinants of elite rowing technique and performance. *Scandinavian Journal of Medicine & Science in Sports*.
Cleary, P. W. (1998). Modelling confined multi-material heat and mass flows using SPH. *Applied Mathematical Modelling, 22*, 981–993.
Cleary, P. W., Cohen, R. C., Harrison, S. M., Sinnott, M. D., Prakash, M., & Mead, S. (2013). Prediction of industrial, biophysical and extreme geophysical flows using particle methods. *Engineering Computations, 30*(2), 157–196.
Cleary, P. W., Pyo, S. H., Prakash, M. and Koo, B. K., (2007b), Bubbling and Frothing Liquids, ACM Transaction on Graphics, 26 (3), Article No. 97.
Cleary, P. W., Ha, J., & Ahuja, V. (2000). High pressure die casting simulation using smoothed particle hydrodynamics. *International Journal of Cast Metals Research, 12*(6), 335–356.
Cleary, P. W., Ha, J., Prakash, M., & Nguyen, T. (2006a). 3D SPH flow predictions and validation for high pressure die casting of automotive components. *Applied Mathematical Modelling, 30*(11), 1406–1427.
Cleary, P. W., & Prakash, M. (2004). Discrete-element modelling and smoothed particle hydrodynamics: Potential in the environmental sciences. *Philosophical Transactions-Royal Society of London Series A Mathematical Physical and Engineering Sciences, 362*, 2003–2030.
Cleary, P. W., Prakash, M., Ha, J., Stokes, N., & Scott, C. (2007a). Smooth particle hydrodynamics: Status and future potential. *Progress in Computational Fluid Dynamics, An International Journal, 7*(2/3/4), 70.
Cleary, P. W., & Rudman, M. (2009). Extreme wave interaction with a floating oil rig: Prediction using SPH. *Progress in Computational Fluid Dynamics, an International Journal, 9*(6), 332–344.
Cleary, P. W., Sinnott, M., & Morrison, R. (2006b). Prediction of slurry transport in SAG mills using SPH fluid flow in a dynamic DEM based porous media. *Minerals Engineering, 19*(15), 1517–1527.
Cleary, P. W., (1996), New implementation of viscosity: tests with Couette flows, SPH Technical Note #8, CSIRO Division of Mathematics and Statistics, Technical Report DMS – C 96/32.
Cohen, R. C. Z., Cleary, P. W., Harrison, S. M., Mason, B. R., & Pease, D. L. (2014). Pitching effects of buoyancy during four competitive swimming strokes. *Journal of Applied Biomechanics, 30*, 609–618.
Cohen, R. C. Z., Cleary, P. W., & Mason, B. R. (2012). Simulations of dolphin kick swimming using smoothed particle hydrodynamics. *Human Movement Science, 31*(3), 604–619.
Cohen, R. C. Z., Cleary, P. W., Mason, B. R., & Pease, D. L. (2015). The role of the hand during freestyle swimming. *Journal of Biomechanical Engineering, 137*(11), 111007.
Cohen, R. C. Z., Cleary, P. W., Mason, B. R., & Pease, D. L. (2018). Forces during front crawl swimming at different stroke rates. *Sports Engineering, 21*(1), 63–73.
Crespo, A. J. C., Gómez-Gesteira, M., & Dalrymple, R. A. (2007). 3D SPH Simulation of large waves mitigation with a dike. *Journal of Hydraulic Research, 45*(5),

631–642.
Cummins, S. J., Silvester, T. B., & Cleary, P. W. (2012). Three-dimensional wave impact on a rigid structure using smoothed particle hydrodynamics. *International Journal for Numerical Methods in Fluids, 68*(12), 1471–1496.
Di Mascio, A., Antuono, M., Colagrossi, A., & Marrone, S. (2017). Smoothed particle hydrodynamics method from a large eddy simulation perspective. *Physics of Fluids, 29*, 035102.
Eddy, A. (2011). Flatwater kayak stroke video.
Farahani, R. J., & Dalrymple, R. A. (2014). Three-dimensional reversed horseshoe vortex structures under broken solitary waves. *Coastal Engineering, 91*, 261–279.
Fry, R., & Morton, A. (1991). Physiological and kinanthropometric attributes of elite flatwater kayakists. *Medicine and Science in Sports and Exercise, 23*(11), 1297–1301.
Gomes, B., Ramos, N., Conceição, F., Vilas-Boas, J. P., Vaz, M. A. P. (2012). Field assessment of the Kayaks' Total Drag Force. In *15th International Conference on Experimental Mechanics*, Porto.
Gomes, B. B., Ramos, N. V., Conceição, F. A. V., Sanders, R. H., Vaz, M. A., & Vilas-Boas, J. P. (2015). Paddling force profiles at different stroke rates in elite sprint kayaking. *Journal of Applied Biomechanics, 31*, 258–263.
Gomes, B., Viriato, N., Sanders, R., Conceição, F., Vaz, M., & Vilas-Boas, J. P. (2011). Analysis of single and team kayak acceleration. *Portuguese Journal of Sport Sciences, 11*(Suppl. 2), 255–257.
Gómez-Gesteira, M., & Dalrymple, R. (2004). Using a three-dimensional smoothed particle hydrodynamics method for wave impact on a tall structure. *Journal of Waterway, Port, Coastal, and Ocean Engineering, 130*(2), 63–69.
Ha, J., & Cleary, P. W. (2000). Comparison of SPH simulations of high pressure die casting with those of Schmidt and Klein. *J. Cast Metals Res. 12*, 409–418.
Ha, J., & Cleary, P. W. (2005). Simulation of high pressure die filling of a moderately complex industrial object using smoothed particle hydrodynamics. *International Journal of Cast Metals Research, 18*(2), 81–92.
Harrison, S. M., & Cleary, P. W. (2014). Towards modelling of fluid flow and food breakage by the teeth in the oral cavity using smoothed particle hydrodynamics (SPH). *European Food Research and Technology, 238*(2), 185–215.
Harrison, S. M., Cohen, R. C. Z., Cleary, P. W., Barris, S., & Rose, G. (2016). A coupled biomechanical-Smoothed Particle Hydrodynamics model for predicting the loading on the body during elite platform diving. *Applied Mathematical Modelling, 40*(5), 3812–3831.
Harrison, S. M., Eyres, G., Cleary, P. W., Sinnott, M. D., Delahunty, C., & Lundin, L. (2014). Computational modeling of food oral breakdown using smoothed particle hydrodynamics. *Journal of Texture Studies, 45*, 97–109.
Helmer, R. J. N., Farouil, A., Baker, J., & Blanchonette, I. (2011). Instrumentation of a kayak paddle to investigate blade/water interactions. *Procedia Engineering, 13*, 501–506.
Jackson, P. S. (1995). Performance prediction for Olympic kayaks. *Journal of Sports Sciences, 13*(3), 239–245.
Jackson, P. S., Locke, N., & Brown, P. (1992). The Hydrodynamics of Paddle Propulsion. In 11th Australasian Fluid Mechanics Conference (pp. 1197–1200).
Janssen, I., & Sachlikidis, A. (2010). Validity and reliability of intra-stroke kayak velocity and acceleration using a GPS-based accelerometer. *Sports Biomechanics, 9*, 47–56.
Jeong, J., & Hussain, F. (1995). On the identification of a vortex. *Journal of Fluid Mechanics, 285*(69), 69–94.
Kavan, L., Collins, S., Zára, J., & O'Sullivan, C. (2008). Geometric skinning with approximate dual quaternion blending. *ACM Transactions on Graphics (TOG), 27*(4), 105.
Kiara, A., Paredes, R., & Yue, D. K. P. (2017). Numerical investigation of the water entry of cylinders without and with spin. *Journal of Fluid Mechanics, 814*, 131–164.
Limonta, E., Squadrone, R., Rodano, R., Marzegan, A., Veicsteinas, A., Merati, G., & Sacchi, M. (2010). Tridimensional kinematic analysis on a kayaking simulator: Key factors to successful performance. *Sport Sciences for Health, 6*(1), 27–34.
Liu, M. B., & Liu, G. R. (2010). Smoothed Particle Hydrodynamics (SPH): An overview and recent developments. *Archives of Computational Methods in Engineering, 17*(1), 25–76.
Mann, R., & Kearney, J. (1979). A biomechanical analysis of the Olympic-style flatwater kayak stroke. *Medicine and Science in Sports and Exercise, 12*(3), 183–188.
McDonnell, L. K., Hume, P. A., & Nolte, V. (2013). A deterministic model based on evidence for the associations between kinematic variables and sprint kayak performance. *Sports Biomechanics, 12*(3), 205–220.
McKean, M. R., & Burkett, B. (2010). The relationship between joint range of motion, muscular strength, and race time for sub-elite flat water kayakers. *Journal of Science and Medicine in Sport, 13*(5), 537–542.
Michael, J. S., Smith, R., & Rooney, K. B. (2009). Determinants of kayak paddling performance. *Sports Biomechanics, 8*(2), 167–179.
Monaghan, J. J. (1994). Simulating free surface flows with SPH. *Journal of Computational Physics, 110*(2), 399–406.
Monaghan, J. J. (2005). Smoothed particle hydrodynamics. *Reports on Progress in Physics, 68*(8), 1703.
Olivier, S. C., & Coetsee, M. F. (2002). Tests for predicting endurance kayak performance. *South African Journal for Research in Sport, Physical Education and Recreation, 24*(2) p–45.
Pan, W., Tartakovsky, A. M., & Monaghan, J. J. (2012). A smoothed-particle hydrodynamics model for ice-sheet and ice-shelf dynamics. *Journal of Glaciology, 58*, 216–222.
Pasculli, A., Minatti, L., Audisio, C., & Sciarra, N. (2014). Insights on the application of some current SPH approaches for the study of muddy debris flow: Numerical and experimental comparison. *Advances in Fluid Mechanics X, 10*, 3.
Prakash, M., Cleary, P. W., Noui-Mehidi, M. N., Blackburn, H., & Brooks, G. (2007). Simulation of suspension of solids in a liquid in a mixing tank using SPH and comparison with physical modeling experiments. *Progress in Computational Fluid Dynamics, 7*, 91–100.
Qiu, Y., Wei, W., Liu, A., & Cao, J. (2008). Comparative research on the stroke rhythm of men and women kayakers in the international competition. In ISBS-Conference Proceedings Archive (Vol. 1).
Robinson, M., Cleary, P. W., & Monaghan, J. J. (2008). Analysis of mixing in a twin-cam mixer using Smoothed Particle Hydrodynamics. *AIChE Journal, 54*, 1987–1998.
Robinson, M., & Monaghan, J. J. (2012). Direct numerical simulation of decaying two-dimensional turbulence in a no-slip square box using smoothed particle hydrodynamics. *International Journal for Numerical Methods in Fluids, 70*, 37–55.
Rudman, M., Cleary, P. W., & Prakash, M. (2009). Simulation of liquid sloshing in model LNG tank using smoothed particle hydrodynamics. *International Journal of Offshore and Polar Engineering, 19*, 286–294.
Sumner, D., Sprigings, E. J., Bugg, J. D., & Heseltine, J. L. (2003). Fluid forces on kayak paddle blades of different design. *Sports Engineering, 6*, 11–19.
Ting, T. S., Prakash, M., Cleary, P. W., & Thompson, M. C. (2006). Simulation of high Reynolds flow over a backward facing step using SPH. *ANZIAM Journal, 47*, C292–C309.
Tzabiras, G. D., Polyzos, S. P., Sfakianaki, K., Diafas, V., Villiotis, A. D., Chrisikopoulos, K., & Kaloupsis, S. (2010). Experimental and numerical study of the flow past the Olympic class k-1 flat water racing kayak at steady speed. *The Sport Journal*.
Van Someren, K., & Howatson, G. (2008). Prediction of flatwater kayaking performance. *International Journal of Sports Physiology and Performance, 3*(2), 207–218.
Van Someren, K., & Palmer, G. S. (2003). Prediction of 200-m Sprint Kayaking Performance. *Canadian Journal of Applied Physiology, 28*(4), 505–517.